A SIMPLIFIED METHOD FOR PREDICTION OF LONG-TERM PRESTRESS LOSS IN POST-TENSIONED CONCRETE BRIDGES

by

SAMER YOUAKIM

VISTASP M. KARBHARI

Department of Structural Engineering
University of California, San Diego
La Jolla, California 92093-0085

July 2006

University of California, San Diego

Department of Structural Engineering

Structural Systems Research Project

Report No. SSRP–06/21

A Simplified Method for Prediction of Long-Term Prestress Loss in Post-Tensioned Concrete Bridges

by

Samer Youakim

Assistant Project Scientist

Vistasp M. Karbhari

Professor of Structural Engineering

Department of Structural Engineering

University of California, San Diego

La Jolla, California 92093-0085

July 2006

1. Report No.	2. Government Accession No.	3. Recipient's Catalog No.

4. Title and Subtitle	5. Report Date
A Simplified Method for Prediction of Long-Term Prestress Loss in Post-Tensioned Concrete Bridges	July 2006
	6. Performing Organization Code

7. Author(s)	8. Performing Organization Report No.
Samer Youakim and Vistasp M. Karbhari	UCSD / SSRP-06/21

9. Performing Organization Name and Address	10. Work Unit No. (TRAIS)
Department of Structural Engineering School of Engineering University of California, San Diego La Jolla, California 92093-0085	
	11. Contract or Grant No.
	59A0337

12. Sponsoring Agency Name and Address	13. Type of Report and Period Covered
California Department of Transportation Engineering Service Center 1801 30th St., West Building MS-9 Sacramento, California 95807	Final Report
	14. Sponsoring Agency Code

15. Supplementary Notes

Prepared in cooperation with the State of California Department of Transportation.

16. Abstract

Creep and shrinkage of concrete and relaxation of prestressing steel cause time-dependent changes in the stresses and strains of concrete structures. These changes result in continuous reduction in the concrete compression stresses and in the tension in prestressing steel. Reasonably accurate estimate of the long-term prestress losses are needed to avoid any serviceability problems of the structure (due to cracking and/or excessive deflection). An analytical method is presented to predict the long-term prestress losses in continuous cast-in-place post-tensioned bridges. The method is based on the basic principles of solid mechanics and satisfies the requirements of equilibrium and compatibility of the bridge cross section. The proposed method for a section in concrete girder reduces to a single equation with three coefficients, which are functions of the modulus of elasticity and creep coefficient of concrete, location and amount of prestressing and non-prestressed steel, and geometry of the cross section. To expedite the use of the method and to make it more appealing to practicing engineers, design aids are provided to estimate these three coefficients. The method is further extended to continuous bridge girders by using the force method to calculate the change in connecting moments at intermediate supports and hence the increase or decrease in prestressing losses. The predictions of the proposed method are compared with the current provisions of design standards and codes of practice. It is shown that the present empirical equations of the bridge standards can overly underestimate or overestimate the long-term prestress losses, depending on the concrete creep and shrinkage properties as well as prestressing and non-prestressed steel ratios.

17. Key Words	18. Distribution Statement
Prestress loss, creep, shrinkage	No restrictions

19. Security Classification (of this report)	20. Security Classification (of this page)	21. No. of Pages	22. Price
Unclassified	Unclassified	72	

Form DOT F 1700.7 (8-72) Reproduction of completed page authorized

Disclaimer

The contents of this report reflect the views of the authors who are responsible for the facts and the accuracy of the data presented herein. The contents do not necessarily reflect the official views or policies of the State of California. This report does not constitute a standard, specification or regulation.

Abstract

Creep and shrinkage of concrete and relaxation of prestressing steel cause time-dependent changes in the stresses and strains of concrete structures. These changes result in continuous reduction in the concrete compression stresses and in the tension in prestressing steel. Reasonably accurate estimate of the long-term prestress losses are needed to avoid any serviceability problems of the structure (due to cracking and/or excessive deflection). An analytical method is presented to predict the long-term prestress losses in continuous cast-in-place post-tensioned bridges. The method is based on the basic principles of solid mechanics and satisfies the requirements of equilibrium and compatibility of the bridge cross section. It is assumed that prestressing and dead load are applied at the same instant, shrinkage starts to take place at the application of loads, and one concrete type for the cross section. The proposed method for a section in concrete girder reduces to a single equation with three coefficients, which are functions of the modulus of elasticity and creep coefficient of concrete, location and amount of prestressing and non-prestressed steel, and geometry of the cross section. To expedite the use of the method and to make it more appealing to practicing engineers, design aids are provided to estimate these three coefficients. The method is further extended to continuous bridge girders by using the force method to calculate the change in connecting moments at intermediate supports and hence the increase or decrease in prestressing losses.

The predictions of the proposed method are compared with the current provisions of design standards and codes of practice. It is shown that the present empirical equations of the bridge standards can overly underestimate or overestimate the long-term prestress losses, depending on the concrete creep and shrinkage properties as well as prestressing and non-prestressed steel ratios. The proposed method is applied to a number of continuous post-tensioned concrete bridges currently under construction in San Diego County. It was found that the prestressing losses due to continuity could be ignored without affecting the accuracy of the method.

Table of Contents

List of Figures

List of Tables

List of Symbols

A = area

B_t/B = ratio of top slab width to bottom slab width

E = modulus of elasticity

$\overline{E}_c(t,t_0)$ = age-adjusted elasticity modulus of concrete

f'_c = concrete compressive strength

f_{cgp} = concrete stress at center of gravity of prestressing steel at transfer

$\overline{f}_{ij}$ = age-adjusted flexibility coefficient. Change in displacement at coordinate i due to unit action applied gradually at coordinate j

f_{pu} = ultimate strength of prestressing steel

f_{py} = yield strength of prestressing steel

f_y = yield strength of non-prestressed steel

h_b/h = ratio of bottom slab thickness to total depth of cross section

h_t/h = ratio of top slab thickness to total depth of cross section

I = second moment of area

l = span length

M = bending moment

N = axial force

PPR = partial prestress ratio

RH = relative humidity (in percent)

t = final time (end of service life of concrete member)

t_s = concrete age at end of curing period, which marks beginning of development of shrinkage strains

V/S = volume-to-surface ratio of concrete member

y = vertical distance measured positive (downwards) from the centroid of the age-adjusted transformed section

α = modular ratio

χ = aging coefficient

χ_r = reduced relaxation coefficient

ΔD = change in angular discontinuity with time

Δf_{cdp} = change in concrete stress at center of gravity of prestressing steel due to permanent loads applied after transfer

ΔF = change in connecting moment with time

$\Delta \varepsilon_c(t, t_0)$ = change in concrete strain between time t_0 and t

$\Delta \varepsilon_O$ = change in axial strain at reference point O

μ = curvature coefficient

$\Delta \sigma_c(t, t_0)$ = stress applied gradually from time t_0 to its full amount at time t

$\Delta \sigma_{pr}$ = intrinsic relaxation

$\Delta \overline{\sigma}_{pr}$ = reduced relaxation

$\Delta \sigma_{ps}$ = total long-term prestress loss

$\Delta \sigma_{ps(cr)}$ = prestress loss due to creep

$\Delta \sigma_{ps(es)}$ = prestress loss due to elastic shortening

$\Delta \sigma_{ps(fr)}$ = prestress loss due to friction

$\Delta \sigma_{ps(sh)}$ = prestress loss due to shrinkage

$\Delta \sigma_{ps(relax)}$ = prestress loss due to relaxation

$\Delta \psi$ = change in curvature

ε_{cs} = shrinkage strain of concrete

$\varepsilon_c(t_0)$ = instantaneous strain at time t_0

$\varepsilon_c(t)$ = total strain at time t

ε_O = axial strain at reference point O

$\varphi(t, t_0)$ = creep coefficient between t_0 and t

$\sigma_c(t_0)$ = stress applied at time t_0 and sustained to a later time t

σ_{p0} = initial stress of prestressing steel

$\sum B_w$ = summation of web thicknesses

ρ = steel ratio

ψ = curvature

Subscripts

c = net concrete section

i = coordinate number (= 1, 2, …) or section integration point (= A, B, …)

ns = non-prestressed steel

ps = prestressing steel

1. Introduction

Creep and shrinkage of concrete and relaxation of prestressing steel cause long-term prestress losses in concrete structures. The effects of these factors are interdependent and it is usually difficult to isolate the effect of each factor. While it is generally accepted that long-term losses do not affect the ultimate capacity of a prestressed concrete member, a reasonably accurate prediction of long-term losses is important to ensure satisfactory performance of the concrete member under service loads. If prestress losses are underestimated, the tensile strength of concrete could be exceeded at critical sections (mid-spans and over supports) under full service loads and thereby causing cracking and large deflections. On the other hand, overestimating prestress losses leads to excessive camber and uneconomic design because of using large amounts of prestressing steel.

The error in predicting the long-term prestress losses can be due to two sources: (1) inaccuracy of the long-term material properties (creep and shrinkage of concrete and relaxation of prestressing steel); and (2) inaccuracy of the method of analysis used. The objective of this report is to address the second source of inaccuracy by presenting a simple, yet comprehensive, analytical method to estimate long-term prestress losses in continuous cast-in-place post-tensioned concrete bridges. The method satisfies the requirements of equilibrium and compatibility of the bridge cross-sections and avoids the use of any empirical equations, as suggested in most bridge codes, which cannot be accurate in all cases. The inaccuracy in the material properties used can be mitigated by varying the input material properties to the proposed method and determine upper and lower bounds on the prestress losses.

2. Long-term Material Properties

2.1 Shrinkage of Concrete

As curing of concrete ends, concrete starts to lose moisture and undergoes change in volume as a result of chemical reactions between cement paste and water. This phenomenon is known as *shrinkage* and it starts to develop rapidly after time t_s, the age of concrete at the end of the curing period, as shown in Fig. 2.1. Shrinkage of concrete ε_{cs} is influenced by the concrete strength f_c' (or concrete mix proportions), the method of curing, the relative humidity of the environment *RH*, the volume-to-surface ratio of the concrete member *V/S* (or the area of the cross section divided by the perimeter exposed to the atmosphere), and the interval of time $t - t_s$.
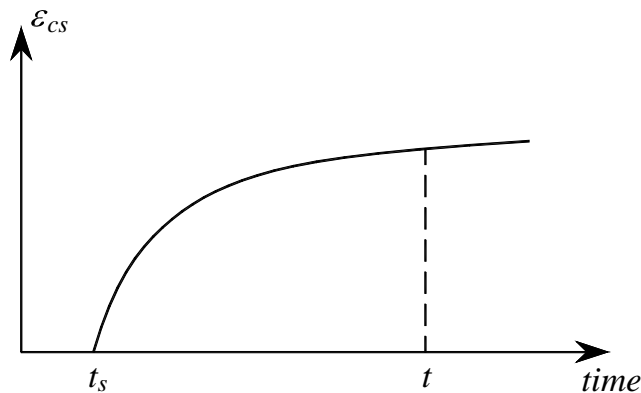
Fig. 2.1 Development of concrete shrinkage with time.

2.2 Creep of Concrete

Creep of concrete is defined as the increase of strain under sustained stress. This increase in strain can be several times the elastic (or instantaneous) strain at first loading. As shown in Fig. 2.2(a), a stress $\sigma_c(t_0)$ is applied at time t_0 and sustained to a later time t, the creep coefficient $\varphi(t, t_0)$ (Fig. 2.2(b)) is defined as the ratio of the creep strain $\varepsilon_c(t) - \varepsilon_c(t_0)$ to the instantaneous strain $\varepsilon_c(t_0)$:

$$\varepsilon_c(t) = \frac{\sigma_c(t_0)}{E_c(t_0)} \left[1 + \varphi(t, t_0)\right] \qquad (2.1)$$

where $E_c(t_0)$ is the modulus of elasticity of concrete at age t_0.

Concrete structures are often subjected to stresses that vary with time from zero at t_0 to some value $\Delta\sigma_c(t, t_0)$ at later time t, as depicted in Fig. 2.2(b). This is typical of some cases such as settlement of supports in continuous concrete beams and long-term prestress losses in prestressed concrete beams. Since the stress in this case is applied gradually, the creep strain at time t will be less than that in the case when stress is applied at full value at time t_0. To account for this, a dimensionless multiplier χ (smaller than unity) referred to as the *aging coefficient* [1,2] is used to express the total strain at time t:

$$\varepsilon_c(t) = \frac{\Delta\sigma_c(t, t_0)}{E_c(t_0)} \left[1 + \chi\, \varphi(t, t_0)\right] \qquad (2.2)$$
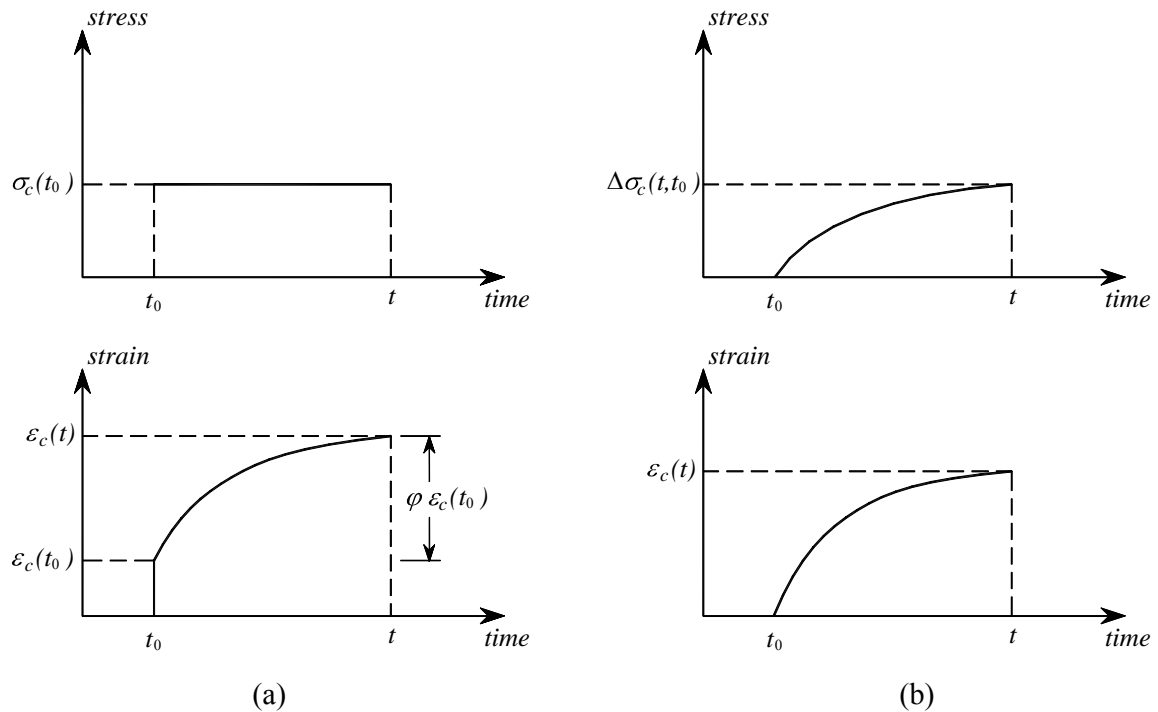
Fig. 2.2 Development of concrete strains with time due to: (a) stress applied at time t_0 and sustained to a later time t; and (b) stress applied gradually from t_0 to t.

The value of χ ranges from 0.6 to 0.9 and depends on the development of $E_c(t)$ with time, the creep coefficient φ, the time period $t - t_0$, and the true shape of $\Delta\sigma_c(t,t_0)$, which is normally not known in advance. For most practical cases, χ can be taken equal to 0.8. It follows from Eq. 2.2 that in the analysis of stresses due to gradually developed forces during a period t_0 to t, $\Delta\sigma_c(t,t_0)$ can be related to the change in strains $\Delta\varepsilon_c(t,t_0)$ using the *age-adjusted elasticity modulus* $\overline{E}_c(t,t_0)$:

$$\overline{E}_c(t,t_0) = \frac{E_c(t_0)}{1 + \chi\varphi(t,t_0)} \tag{2.3}$$

Creep is influenced by the same factors that affect shrinkage in addition to the age of concrete at loading. It is generally accepted that for stress levels below $0.4\,f_c'$, which is the common range of concrete stresses at service conditions, the creep coefficient φ is independent of the applied stress. For most practical situations, φ varies between 2 and 4.

2.3 Relaxation of Prestressing Steel

Similar to concrete, prestressing steel subjected to stresses more than 50% of its ultimate strength f_{pu} exhibits some creep. In practice, steel used for prestressing is usually subjected to stresses between 0.5 to 0.8 of its ultimate strength. When a prestressing tendon is stretched between two points, it will be subjected to a constant strain. Because of creep, the stress in the tendon decreases (or relaxes) with time to maintain the state of constant strain. This reduction in stress is known as *intrinsic relaxation* $\Delta\sigma_{pr}$. It depends on the type of prestressing tendons (stress relieved or low-relaxation), the ratio of the initial stress σ_{p0} to the yield stress f_{py} and the time t from initial stressing. An equation that is widely used in North America[3] for $\Delta\sigma_{pr}$ in low-relaxation strands is given by

$$\Delta\sigma_{pr} = \frac{\log(24t)}{40}\left(\frac{\sigma_{p0}}{f_{py}} - 0.55\right)\sigma_{p0} \tag{2.4}$$

In prestressed concrete members, the two ends of the prestressing tendons constantly move toward each other because of the creep and shrinkage effects of concrete, thereby reducing the tensile stress in the tendons. This reduction in tension has a similar effect as if the tendons were subjected to lesser initial stress. Thus, a reduced relaxation value $\Delta\overline{\sigma}_{pr}$ has to be used in the analysis of long-term effects in prestressed members:

$$\Delta\overline{\sigma}_{pr} = \chi_r \ \Delta\sigma_{pr} \tag{2.5}$$

where χ_r is a dimensionless coefficient less than unity. Ghali and Trevino[4] presented a graph to evaluate χ_r that depends on, among other factors, the total prestress loss $\Delta\sigma_{ps}$. Since $\Delta\sigma_{ps}$ is not known in advance, normally a trial and error procedure is required. A common value for χ_r that is used in practice is 0.7.

3. Provisions of Bridge Codes for Long-term Prestress Losses

3.1 AASHTO-LRFD Refined Method[5]

The total long-term prestress loss $\Delta\sigma_{ps}$ is expressed as the summation of prestress loss due to creep $\Delta\sigma_{ps(cr)}$, prestress loss due to shrinkage $\Delta\sigma_{ps(sh)}$, and prestress loss due to relaxation $\Delta\sigma_{ps(relax)}$, as follows:

$$\Delta\sigma_{ps(cr)} = 12 f_{cgp} - 7\Delta f_{cdp} \tag{3.1}$$

$$\Delta\sigma_{ps(sh)} = (13.5 - 0.123RH) \tag{3.2}$$

$$\Delta\sigma_{ps(relax)} = 0.3\{20 - 0.3\Delta\sigma_{ps(fr)} - 0.4\Delta\sigma_{ps(es)} - 0.2(\Delta\sigma_{ps(sh)} + \Delta\sigma_{ps(cr)})\} \tag{3.3}$$

where

f_{cgp} = concrete stress at center of gravity of prestressing steel at transfer;

Δf_{cdp} = change in concrete stress at center of gravity of prestressing steel due to permanent loads applied after transfer;

RH = relative humidity in percent; and

$\Delta\sigma_{ps(fr)}$ and $\Delta\sigma_{ps(es)}$ = prestress losses due to friction and elastic shortening, respectively.

3.2 AASHTO-LRFD Approximate Method[5]

For post-tensioned concrete bridges with spans up to 160 ft (50 m), stressed at concrete age of 10 to 30 days with low-relaxation strands and subjected to average exposure conditions, the following equations are given by AASHTO-LRFD for box girder bridges:

$$\Delta\sigma_{ps} = 17 + 4PPR \text{ (Upper bound)} \tag{3.4}$$

$$\Delta\sigma_{ps} = 15 + 4PPR \text{ (Average)} \tag{3.5}$$

PPR is the partial prestress ratio given by:

$$PPR = \frac{A_{ps}f_{py}}{A_{ps}f_{py} + A_s f_y} \tag{3.6}$$

where

A_{ps} and A_s = area of prestressing and non-prestressed steel, respectively; and

f_{py} and f_y = yield strength of prestressing and non-prestressed steel, respectively.

3.3 CEB-FIP Model Code[6]

The following equation was suggested to estimate the long-term prestress losses:

$$\Delta\sigma_{ps} = \frac{\alpha_{ps}\varphi(t,t_0)f_{cgp} + E_{ps}\varepsilon_{cs} + 0.8\Delta\sigma_{pr}}{1 + \alpha_{ps}\dfrac{A_{ps}}{A_c}\left(1 + \dfrac{A_c y_{ps}^2}{I_c}\right)(1 + \chi\varphi(t,t_0))} \tag{3.7}$$

where

$\alpha_{ps} = E_{ps}/E_c$ = ratio of modulus of elasticity of prestressing steel to that of concrete;

A_{ps} and A_c = areas of prestressing steel and net concrete section, respectively;

I_c = second moment of area of net concrete section; and

y_{ps} = y-coordinate of prestressing steel measured downwards from centroid of net concrete section.

Equation 3.7 was derived assuming a single layer of prestressing steel; the effect of non-prestressed steel was not taken into account. The reduced relaxation coefficient χ_r (see Eq. 2.5) was taken 0.8.

3.4 Canadian Highway Bridge Design Code[7] (CHBDC)

For post-tensioned concrete bridges with low-relaxation strands and A_s/A_{ps} ratio less than unity, CHBDC recommends the use of the following equations:

$$\Delta\sigma_{ps(cr)} = 1.6\left[1.37 - 0.77(0.01RH)^2\right]\alpha_{ps}(f_{cdg} - f_{cdp}) \tag{3.8}$$

$$\Delta\sigma_{ps(sh)} = 13.6 - 0.12RH \tag{3.9}$$

$$\Delta\sigma_{ps(relax)} = \left(\frac{\sigma_{p0}}{f_{pu}} - 0.55\right)\left(0.34 - \frac{\Delta\sigma_{ps(cr)} + \Delta\sigma_{ps(sh)}}{1.25 f_{pu}}\right)\frac{f_{pu}}{3} \geq 0.002 f_{pu} \tag{3.10}$$

4. Proposed Method of Analysis

4.1 Assumptions

- One layer of prestressing steel

- One concrete type for the entire cross section

- Any cross-sectional shape

- Prestressing and dead load are applied at the same time t_0 to the concrete section (this may not reflect normal construction operations and will be researched at a later date)

- The wearing surface load is ignored or could be considered at an earlier time t_0

- Assume the prestressing is applied at the same time of end of curing of concrete; i.e., shrinkage will start to take place at $t_s = t_0$.

4.2 Sign Convention

The following sign convention will be used throughout the report. Axial force N is positive when it is tensile. Bending moment M and its associated curvature ψ are positive when they produce tension at the bottom fiber of the cross section. Stress σ and strain ε are positive when they produce tension. Positive vertical distance y from the centroid of the cross section is measured downward. It follows that the concrete shrinkage, ε_{cs}; the reduced steel relaxation, $\Delta\bar{\sigma}_{pr}$; and the total prestress loss, $\Delta\sigma_{ps}$, are always negative quantities. However, for convenience of illustration, the absolute value of $\Delta\sigma_{ps}$ will be used in graphs.

4.3 Steps of Analysis

The procedure of time-dependent analysis of a concrete section can be summarized in four steps,[8] as shown in Fig. 4.1.

Step 1:

Determine the distribution of instantaneous strain at time t_0 due to dead load and prestressing force after immediate losses (friction, anchorage slip and elastic shortening).

The distribution of strain can be defined by the strain at an arbitrary point O, $\varepsilon_O(t_0)$ and the curvature $\psi(t_0)$. The transformed section properties at time t_0 should be used. Since at this stage the prestressing steel is not yet bonded to concrete, its area should not be included in the analysis. Note that the assumption of introducing the prestressing and dead load at the same instant is fairly acceptable since prestressing causes the member to camber and the gap that forms between the member and formwork is usually sufficient to activated the dead load.
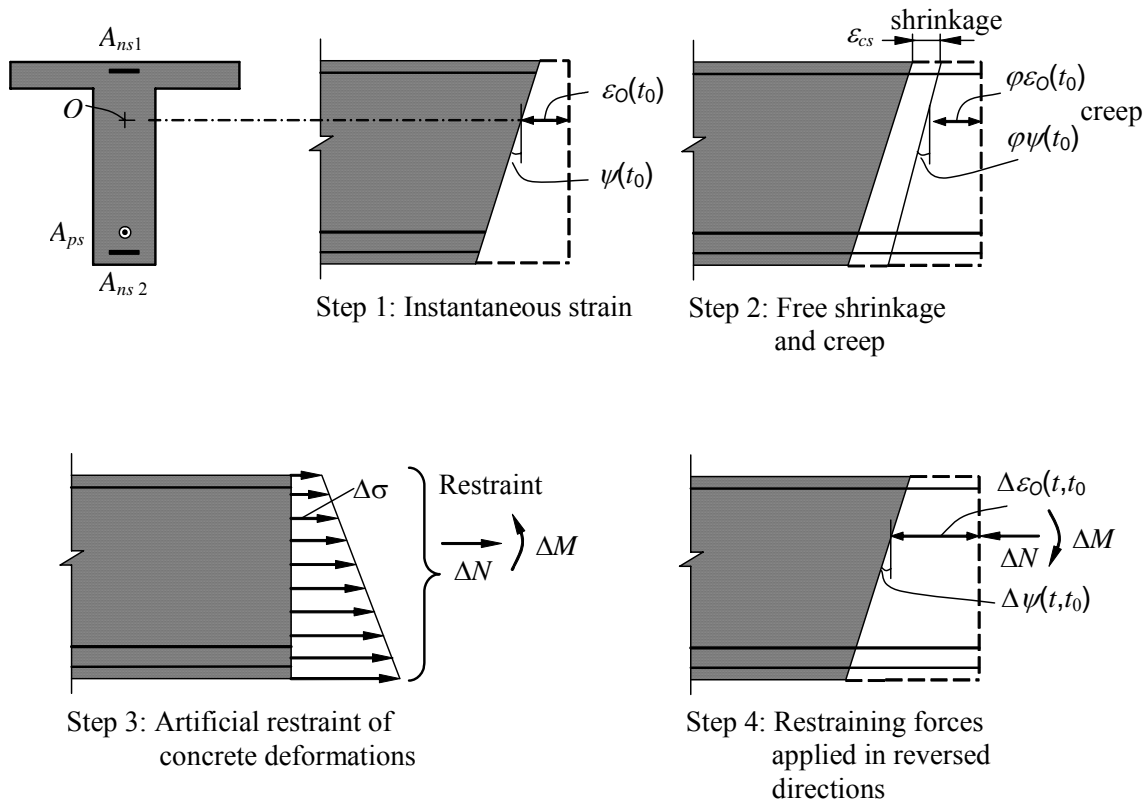
Fig. 4.1 Four steps for the analysis of time-dependent effects (after Ghali et al. 2002).

Step 2:

Determine the hypothetical change in strain distribution in the period t_0 to t due to creep and shrinkage. The change in strain is $\varphi\varepsilon_O(t_0)+\varepsilon_{cs}$ and the change in curvature is $\varphi\psi(t_0)$.

Step 3:

Apply artificial restraining stresses gradually on the cross section during the period t_0 to t to counteract the hypothetical strains calculated in Step (2). The restraining stress $\Delta\sigma_{restrained}$ at any fiber y can be calculated by

$$\Delta\sigma_{restrained} = -\overline{E}_c\{\varphi[\varepsilon_O(t_0)+\psi(t_0)y]+\varepsilon_{cs}\} \tag{4.1}$$

where $\overline{E}_c$ is given by Eq. 2.3. Note that $\Delta\sigma_{restrained}$ is applied only on the net concrete section. The change in concrete strains due to relaxation of prestressing steel can be artificially prevented by application of a force equal to $A_{ps}\overline{\sigma}_{pr}$ at the centroid of prestressing steel.

Step 4:

Integrate the artificial stresses determined in Step 3 to get a normal force ΔN and a moment ΔM at point O. To eliminate the artificial restraint, apply ΔN and ΔM in reversed direction on the age-adjusted transformed section to determine the long-term changes in strains and curvatures of the cross section. Since the prestressing ducts are shortly grouted after prestress transfer, the properties of the cross section include the area of the prestressing steel at this stage.

4.4 Derivation of Method of Analysis

In the four steps presented in the previous section, an arbitrary reference point O was selected to perform all the calculations. This is most suited for computer programming and for structures built in stages; however, the equations become quite involved since point O is not the centroid of the cross section. Since the objective of this report is to present a method that is simple enough for use by practicing engineers, the centroid of the cross section will be determined in each step.

(a) Step 1: Instantaneous strains

Determine the instantaneous strain and curvature at time t_0 due to the dead load and prestressing forces after immediate losses:

$$\varepsilon_{O_1}(t_0) = N_{equivalent}\big/[E_c(t_0)A] \; ; \; \psi(t_0) = M_{equivalent}\big/[E_c(t_0)I] \tag{4.2}$$

where

O_1 = centroid of transformed section at time t_0;

$N_{equivalent}$ = equivalent normal force due to dead weight and prestressing;

$M_{equivalent}$ = equivalent moment due to dead load and prestressing at centroid of the transformed section at time t_0;

$\varepsilon_{O_1}(t_0)$ = axial strain at O_1 due to applied loads at time t_0;

$\psi(t_0)$ = curvature due to applied loads at time t_0;

A = area of the transformed section at time t_0;

I = second moment of area of the transformed section at time t_0 about O_1; and

$E_c(t_0)$ = modulus of elasticity of concrete at time t_0.

Since only single layer of prestressing is assumed, the elastic deformation of concrete takes place when the jacking force is applied, and there is automatic compensation for the elastic shortening loss. The steel stress in prestressing steel immediately after transfer is equal to the initial stress minus the immediate losses (friction plus anchorage slip).
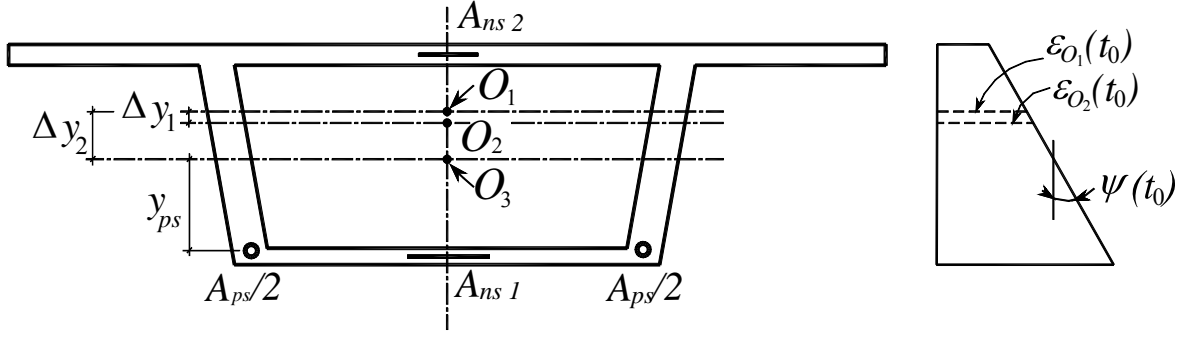
O_1 (Centroid of transformed area at time t_0)
O_2 (Centroid of net concrete section)
O_3 (Centroid of age-adjusted transformed section)

Fig. 4.2 Typical strain distribution in a bridge girder at transfer.

(b) Step 2: Free creep and shrinkage of concrete

Determine the axial strain at the centroid of the net concrete section O_2 :

$$\varepsilon_{O_2}(t_0) = \varepsilon_{O_1}(t_0) + \psi(t_0)\,\Delta y_1 \tag{4.3}$$

where Δy_1 = vertical distance between O_1 and O_2. For most practical applications, Δy_1 is very small compared to the section depth h and can be neglected: $\varepsilon_{O_2} \approx \varepsilon_{O_1}$. The hypothetical change in strain and curvature would be $\varphi\varepsilon_{O_2}(t_0) + \varepsilon_{cs}$ and $\varphi\psi(t_0)$.

(c) Step 3: Calculation of artificial force necessary to prevent creep and shrinkage

Calculate artificial forces ΔN and ΔM at the centroid of the net concrete section O_2 necessary to prevent free creep and shrinkage:

$$\Delta N_{creep} = -\overline{E}_c\,\varphi A_c\,\varepsilon_{O_2}(t_0) ; \quad \Delta M_{creep} = -\overline{E}_c\,\varphi I_c\,\psi(t_0) \tag{4.4}$$

$$\Delta N_{shrinkage} = -\overline{E}_c\,\varepsilon_{cs}\,A_c \tag{4.5}$$

$$\Delta N = -\overline{E}_c A_c\left[\varphi\,\varepsilon_{O_2}(t_0) + \varepsilon_{cs}\right] \tag{4.6}$$

$$\Delta M = -\overline{E}_c\,I_c\,\varphi\,\psi(t_0) \tag{4.7}$$

where

A_c = area of the net concrete section;

I_c = second moment of area of the net concrete section about O_2;

$\overline{E}_c$ = age-adjusted elasticity modulus of concrete = $E_c(t_0)/(1 + \chi\varphi)$;

χ = aging coefficient;

φ = creep coefficient between t_0 and t; and

ε_{cs} = shrinkage strain between t_0 and t.

(d) Step 4: Application of the artificial forces in reversed direction

Transfer ΔN and ΔM from O_2 to the centroid of the age-adjusted transformed section O_3:

$$\Delta N^* = \Delta N \tag{4.8}$$

$$\Delta M^* = \Delta M - \Delta N(\Delta y_2 - \Delta y_1) \tag{4.9}$$

Δy_2 = vertical distance between O_1 and O_3 (usually positive value for a section at midspan). Usually Δy_1 is very small compared to Δy_2: $\Delta y = \Delta y_2 - \Delta y_1 = \Delta y_2$

$$\Delta M^* = \Delta M - \Delta N \,\Delta y \tag{4.10}$$

Apply ΔN^* and ΔM^* in reversed direction on the age-adjusted transformed section:

$$\Delta\varepsilon_O = -\Delta N^* / (\overline{E}_c \overline{A}) \tag{4.11}$$

$$\Delta\psi = -\Delta M^* / (\overline{E}_c \overline{I}) \tag{4.12}$$

where

$\overline{A}$ = area of the age-adjusted transformed section;

$\overline{I}$ = second moment of area of the age-adjusted transformed section;

$\Delta\varepsilon_O$ = change in the axial strain between t_0 and t at O_3; and

$\Delta\psi$ = change in curvature between t_0 and t

Substituting from Eqs. 4.6 through 4.10, $\Delta\varepsilon_O$ and $\Delta\psi$ can be expressed as:

$$\Delta\varepsilon_O = k_A \,\Delta\varepsilon_{free} \tag{4.13}$$

$$\Delta\psi = k_I \Delta\psi_{free} - k_h \,\Delta\varepsilon_{free}/h \tag{4.14}$$

where

$$k_A = \frac{A_c}{A}; \quad k_I = \frac{I_c}{I}; \quad k_h = \frac{A_c \, \Delta_y \, h}{\bar{I}} \tag{4.15}$$

$$\Delta \varepsilon_{free} = \varphi \, \varepsilon_{O_2}(t_0) + \varepsilon_{cs}; \quad \Delta \psi_{free} = \varphi \, \psi(t_0) \tag{4.16}$$

The long-term prestress loss $\Delta \sigma_{ps}$ between t_0 and t can be given by

$$\Delta \sigma_{ps} = E_{ps} \left[\Delta \varepsilon_O + \Delta \psi \, y_{ps} \right] \tag{4.17}$$

$$\Delta \sigma_{ps} = E_{ps} \left\{ k_A \, \Delta \varepsilon_{free} + y_{ps} \left[k_I \Delta \psi_{free} - k_h \Delta \varepsilon_{free} / h \right] \right\} \tag{4.18}$$

where y_{ps} = y-coordinate of prestressing steel with respect to the centroid of the age-adjusted transformed section O_3 (Fig. 4.2).

4.5 Prestress Loss Due to Relaxation

Following the same procedure to evaluate prestressing losses due to creep and shrinkage, the prestress loss due to relaxation can be determined. The artificial forces to be applied at the centroid of the age-adjusted transformed section O_3 to prevent relaxation of prestressing steel:

$$\{\Delta N\}_{relax} = A_{ps} \, \Delta \bar{\sigma}_{pr}; \quad \{\Delta M\}_{relax} = A_{ps} \, y_{ps} \, \Delta \bar{\sigma}_{pr} \tag{4.19}$$

Apply the artificial forces in reversed direction on the age-adjusted transformed section to evaluate the change in axial strain $(\Delta \varepsilon_O)_{relax}$ and curvature $(\Delta \psi)_{relax}$ due to relaxation:

$$\Delta \varepsilon_O = \frac{-A_{ps} \, \Delta \bar{\sigma}_{pr}}{\bar{E}_c \bar{A}}; \quad \Delta \psi = \frac{-A_{ps} \Delta \bar{\sigma}_{pr} y_{ps}}{\bar{E}_c \bar{I}} \tag{4.20}$$

The long-term prestress loss due to relaxation $(\Delta \sigma_{ps})_{relax}$ can be computed as

$$\Delta \sigma_{ps(relax)} = \Delta \bar{\sigma}_{pr} \left[1 - \frac{E_{ps}}{\bar{E}_c} \left(\frac{A_{ps}}{\bar{A}} + \frac{A_{ps} y_{ps}^2}{\bar{I}} \right) \right] \tag{4.21}$$

Equation 4.21 can be rewritten as

$$\Delta \sigma_{ps(relax)} = \Delta \bar{\sigma}_{pr} \left[1 - \frac{E_{ps}}{\bar{E}_c} \left(k_{Aps} + k_y \right) \right] \tag{4.22}$$

where

$$k_{Aps} = \frac{A_{ps}}{\bar{A}} \; ; \; k_y = \frac{A_{ps} y_{ps}^2}{\bar{I}} \qquad (4.23)$$

For all practical applications (see survey in Sec. 4.6), the term $\left[1 - \frac{E_{ps}}{\bar{E}_c} \left(k_{Aps} + k_y \right) \right]$ was

found to vary within a narrow range between 0.98 and 0.69. Therefore, an average value of 0.85 can be assumed without sacrificing the accuracy of the method:

$$\Delta\sigma_{ps(\,relax\,)} = 0.85 \Delta\bar{\sigma}_{pr} \qquad (4.24)$$

4.6 Design Aids

To evaluate the long-term prestress loss $\Delta\sigma_{ps}$, the terms $\Delta\varepsilon_{free}$ and $\Delta\psi_{free}$ (Eq. 4.16) can be easily determined: $\varepsilon_{O_2}(t_0)$ and $\psi(t_0)$ can be calculated from the initial loading conditions; φ and ε_{cs} can be estimated from any design standards, such as ACI 209[9] and CEB-FIP MC-90.[6] The coefficients k_A, k_I, and k_h can be calculated from the geometric dimensions, prestressing and non-prestressed steel ratios and the creep coefficient of the cross section or by using design aids, as will be illustrated in the following.
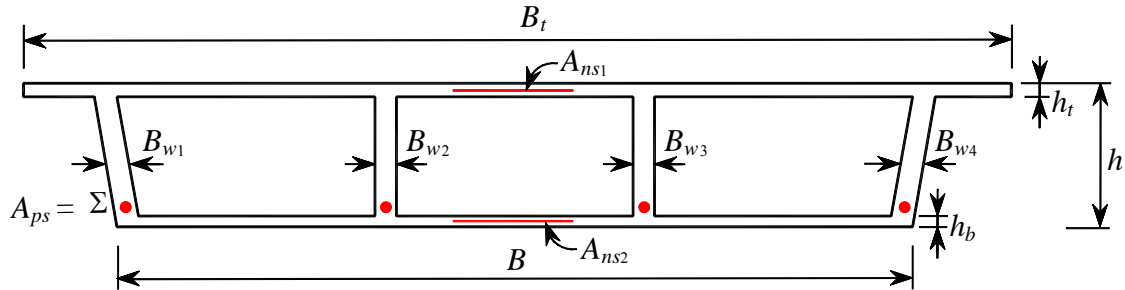
Fig. 4.3 Geometric dimensions and reinforcement in a typical bridge cross section.

Fig. 4.3 shows a typical cross section of a post-tensioned box girder bridge. The number of cells in the figure is chosen arbitrary. The geometric dimensions are defined in Fig. 4.3. Note that the widths of the inclined external webs (B_{w1} and B_{w4}) have to be measured parallel to the horizontal. To be able to determine the practical range of variation of these variables, a survey of bridges currently under construction or soon to be

constructed in California was conducted. Table 4.1 summarizes the results of the survey, where:

$\Sigma B_w = B_{w1} + B_{w2} + ... =$ summation of web widths of the cross section;

$\rho_{ns1} = A_{ns1}/B_t \, h_t =$ ratio of non-prestressed steel in top slab;

$\rho_{ns2} = A_{ns2}/B \, h_b =$ ratio of non-prestressed steel in bottom slab; and

$\rho_{ps} = A_{ps}/h \, \Sigma B_w =$ ratio of prestressing steel with respect to web areas.

Table 4.1 Survey of bridges under construction in the State of California

Variable	Range	Selected values in parametric studies
No. of cells	2 ~ 10	Any number of cells
Span length	26 ~ 80 m	N/A
$\Sigma B_w/B$	0.1 ~ 0.3	0.1, 0.2, 0.3
h_t/h	0.05 ~ 0.15	0.05, 0.10, 0.15
h_b/h	0.05 ~ 0.20	0.05, 0.10, 0.15
B_t/B	1.0 ~ 2.0	1.0, 1.5, 2.0
ρ_{ns1}	0.5% ~ 3.0%	0.2, 1.5, 3.0%
ρ_{ns2}	0.2% ~ 1.6%	0.2, 1.5, 3.0%
ρ_{ps}	0.8% ~ 1.0%	0.8, 1.2%
RH	40% ~ 90%	40% − 90%
V/S	5 ~ 7 in. (130 − 180 mm)	5, 7 in. (130, 180 mm)
$\chi\varphi$	1 ~ 3	1, 2, 3
ε_{sc}	200 ~ 600 × 10^{-6}	500 × 10^{-6}

The National Oceanic and Atmospheric Administration (NOAA) provides, through its web site, statistical data about the monthly and average annual relative humidity *RH*

values (morning and afternoon) for major cities and resorts in the United Sates.[10] For the State of California, the lowest average annual *RH* was reported in Bakersfield (39% in the afternoon); Santa Maria has the highest *RH* (87% in the morning). Therefore, a range for *RH* between 40% to 90% was considered. It should be mentioned that *RH* values as low as 20% were reported for the community of Bishop but was excluded from the study for scarce bridge construction in this area.

In order to determine the common range of *V/S* ratios for post-tensioned bridges in California, typical bridge cross sections for spans between 26 and 80 m were assumed. The number of cells varied between 2 and 10; the overhang slab was either taken equal to 4 ft (1200 mm) or 6.5 ft (2000 mm). The bridge dimensions for each span range were taken similar to respective bridges currently under construction. As per AASHTO-LRFD recommendations for poorly ventilated enclosed cells (Article 5.4.2.3.2), only 50% of the interior perimeter is used in calculating the surface area *S*. The *V/S* ratio was found to vary between 5 in. (130 mm) and 7 in. (180 mm). The *RH* and *V/S* ratios were used to determine the upper and lower bound values of the creep coefficient φ (and accordingly $\chi\varphi$) and the shrinkage coefficient ε_{sc} listed in Table 4.1 using varies the empirical models included in ACI 209,[9] CEB-FIP MC-90,[6] AASHTO-LRFD,[5] and NCHRP Report 496.[11]

A spreadsheet was developed to calculate the variation of the coefficients k_A, k_I, and k_h with $\chi\varphi$ for each of the selected geometric dimensions and steel ratios listed in Table 4.1. The following two assumptions were made: (1) $A_{ns1} = A_{ns2}$ and their centroids are located at mid-depth of the top and bottom flanges, respectively; and (2) depth of prestressing steel $d_{ps} = 0.8h$ (for section at mid-span) and $= 0.2h$ (for section at support). The coefficients k_A, k_I, and k_h are presented in graphs in Appendix A. It should be noted that for some graphs, for clarity of presentation, the upper and lower bound values of a specific variable were only used instead of the entire range listed in Table 4.1; linear interpolation can be used for intermediate values not shown in the graphs.

4.7 Effect of Continuity

Consider a two-span continuous beam, as shown in Fig. 4.4. The variation of the tendon profile is parabolic in each span. Other assumptions are as listed in Sec. 4.1. Solve the statically indeterminate beam by any method of structural analysis (such as force method) to determine the moment diagram at time t_0 due to dead load and prestressing (after immediate losses).
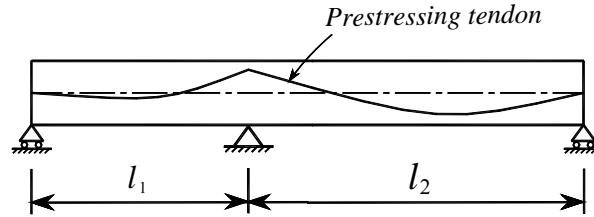
Fig. 4.4 Two-span continuous prestressed beam.

Perform the time-dependant sectional analysis as shown previously in Sec. 4.4 for each of the three sections shown in Fig. 4.5 and determine $(\Delta \psi)_i$ for each section, where $i = A, B$ and C.
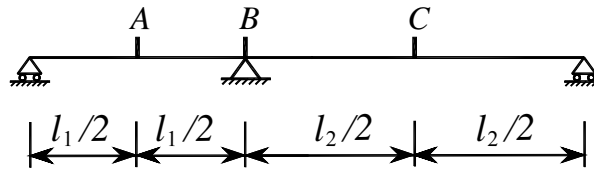
Fig. 4.5 Locations of integration points (sections) in a two-span beam.

Use the force method to determine the change in internal forces and displacements in the continuous beam. The released structure in Fig. 4.6 with the shown coordinate system shown can be used. Assume the change in angular discontinuity at middle support between t_0 and t is ΔD_1 and the unknown change in the connecting moment is ΔF_1. The change in angular discontinuity ΔD_1 can be evaluated as the summation of the two end rotations of each of the simple spans l_1 and l_2. Using the method of elastic weights and assuming parabolic variation of curvature in each span, ΔD_1 can be expressed as[12]

$$\Delta D_1 = \frac{l_1}{6}\left[2(\Delta \psi)_A + (\Delta \psi)_B\right] + \frac{l_2}{6}\left[2(\Delta \psi)_C + (\Delta \psi)_B\right] \qquad (4.25)$$
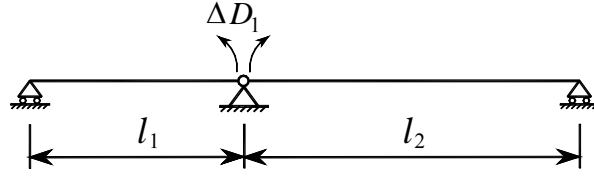
Fig. 4.6 Released structure and coordinate system for a two-span beam.

Due to unit load of the connecting moment $\Delta F_1 = 1$ that is to be applied gradually on the released structure from zero at time t_0 to unity at time t (Fig. 4.7), determine the change in curvature at each section $(\Delta \psi_{u1})_i$:

$$(\Delta \psi_{u1})_i = -(\Delta F_1)_i / (\overline{E_c \overline{I}})_i \tag{4.26}$$
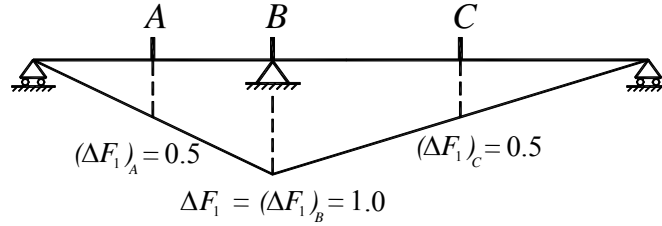
Fig. 4.7 Moment diagram due to unit value of connecting moment.

Evaluate the age-adjusted flexibility coefficient $\overline{f}_{11}$:

$$\overline{f}_{11} = \frac{l_1}{6}\left[2(\Delta \psi_{u1})_A + (\Delta \psi_{u1})_B\right] + \frac{l_2}{6}\left[(2(\Delta \psi_{u1})_C + (\Delta \psi_{u1})_B\right] \tag{4.27}$$

The change in connecting moment ΔF_1 can be computed by solving the compatibility equation $\overline{f}_{11}\Delta F_1 + \Delta D_1 = 0$:

$$\Delta F_1 = \frac{-\Delta D_1}{\overline{f}_{11}} \tag{4.28}$$

The prestress loss at each section due to continuity at each section $(\Delta \sigma_{ps(cont)})_i$ can be given by

$$(\Delta \sigma_{ps(cont)})_i = \left(\frac{E_{ps}}{\overline{E}_c}\right)\left(\frac{\Delta F_1}{\overline{I}} y_{ps}\right)_i \tag{4.29}$$

19

where $\left(\Delta F_1\right)_i$ is the change in moment at each section. For instance, $\left(\Delta F_1\right)_A = \left(\Delta F_1\right)_B = \Delta F_1/2$.

5. Comparisons with Bridge Design Specifications

A brief summary of the current design equations for long-term prestress losses was given in Section 3. Most specifications give separate equations for each prestress loss component due to creep, shrinkage, and relaxation. Therefore, the predictions of the proposed method will be compared with the design equations for prestress loss due to each component individually; the comparison for total prestress loss is presented afterwards. For low-relaxation strands, the long-term prestress loss due to relaxation is usually a small quantity of the total prestress loss and, therefore, will only be included (using Eq. 4.22) in the comparison for total prestress losses. In Eq. 4.22, $\Delta\overline{\sigma}_{pr}$ was evaluated from Eq. 2.7 with $\Delta\sigma_{pr}$ and χ_r taken equal to 3 ksi and 0.8, respectively. In the proposed method, the prestress loss due to creep $\Delta\sigma_{ps(cr)}$ and due to shrinkage $\Delta\sigma_{ps(sh)}$ can be given, respectively, by substituting ε_{cs} and φ equal to zero in Eq. 4.18:

$$\Delta\sigma_{ps\,(cr)} = E_{ps}\left\{k_A\,\varepsilon_O + y_{ps}\left[k_I\,\psi(t_0) - k_h\frac{\varepsilon_O}{h}\right]\right\}\varphi \tag{5.1}$$

$$\Delta\sigma_{ps(sh)} = E_{ps}\left\{k_A - y_{ps}\frac{k_h}{h}\right\}\varepsilon_{cs} \tag{5.2}$$

In all of the comparisons presented in this chapter, the following geometric properties of the bridge cross-section are assumed: $\Sigma B_w/B = 0.2$; $B_t/B = 1.5$; and $h_t/h = h_b/h = 0.1$. The depth of the prestressing steel d_{ps} is assumed $0.8h$ and centroids of the non-prestressed steel in top and bottom slabs are assumed at mid-slab depth. The coefficients k_A, k_I and k_h can be evaluated from either Eq. 4.15 or from the graphs in Appendix A.

5.1 AASHTO-LRFD Refined and Approximate Methods

The AASHTO-LRFD refined method for prestress loss due to creep (Eq. 3.1) is a function of the concrete stress at the center of gravity of prestressing tendons at transfer f_{cgp} and the elastic stress due to additional permanent loads applied after transfer Δf_{cdp}. For post-tensioned bridges, almost all the permanent loads (the dead weight of the bridge

and the prestressing) are introduced at transfer. The wearing surface may never be applied, or if applied that would after long time when most of the long-term deformations have taken place. Therefore, the term Δf_{cdp} is taken equal to zero and Eq. 3.1 reduces to

$$\Delta\sigma_{ps\,(cr)} = 12 f_{cgp} \tag{5.3}$$

To be able to compare Eq. 5.3 with the proposed method, two stress profiles across the depth of the section at transfer have been assumed, as shown in Fig. 5.1. At transfer, the AASHTO-LRFD limits the compression stress at bottom fiber to $0.55 f_{ci}$ and permits no tensile stresses at top fiber. These stress limits were used for stress profile (1) (Fig. 5.1(a)) assuming a specified concrete strength f_c' at 28 days of 4.35 ksi (30 MPa). The concrete strength at transfer f_{ci} was taken $0.7 f_c'$. In the stress profile (2) shown in Fig. 5.1(b), the concrete stress at the center of gravity of prestressing steel was kept the same (1.33 ksi), but a compression stress of 0.46 ksi ($0.15 f_{ci}$) was assumed at the top fiber. It is believed that stress profiles (1) and (2) represent common boundary limits for stress states at transfer. Strain profiles (1) and (2) are obtained from their respective stress profiles by dividing by the concrete modulus of elasticity at transfer.
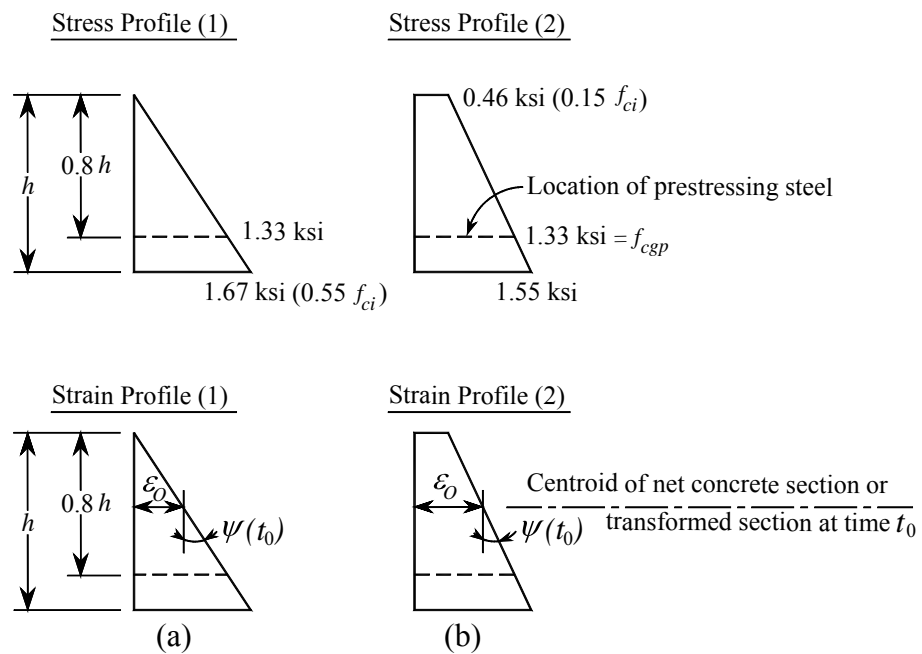

Fig. 5.1 Assumed stress and strain profiles at time of transfer.

The predictions of the proposed method and AASHTO-LRFD refined method for long-term prestress losses due to creep are compared in Figs. 5.2(a) and (b) for prestressing steel ratios of 0.8% and 1.2%, respectively. The independent variable was chosen to be $\chi\varphi$. The aging coefficient χ is assigned a constant value of 0.8; therefore, variation in $\chi\varphi$ essentially reflects variation in φ. The effect of the non-prestressed steel is studied by assuming ratios of ρ_{ns}, equal to 0.2%, 1.5%, and 3.0%, for each strain profile.

As shown in Fig. 5.2, the AASHTO prediction is a straight horizontal line since it is only a function of the concrete stress at the center of gravity of prestressing steel (Eq. 5.3). Compared with the proposed method, the AASHTO prediction changes from underestimating to overestimating creep losses as the creep coefficient increases. The AASHTO equation does not take into account the effect of non-prestressed steel. While this could be acceptable for pretensioned girders since they contain little or no such reinforcement, this cannot be neglected in post-tensioned bridges. As can be seen in Fig. 5.2, the effect of non-prestressed steel reduces the absolute value of prestress loss.

Among other factors, the long-term prestress loss due to creep is dependent on the strain profile of the concrete cross section at time t_0 (application of post-tensioning and dead weight). The strain profile can be determined by the strain at an arbitrary reference point $\varepsilon_O(t_0)$ and the slope of the strain profile $\psi(t_0)$. The AASHTO-LRFD refined method (Eq. 5.3) is a function of the concrete stress (and hence the concrete strain) at the centroid of prestressing steel and therefore recognizes only the effect of the first parameter. As can be seen from both parts in Fig. 5.2, changing the strain profile results in insignificant variation in the prestress loss. It appears that increasing the strain at the net concrete section $\varepsilon_O(t_0)$ in strain profile (2) is offset by its reduced slope $\psi(t_0)$ (see Eq. 5.1).

Increasing the ratio of prestressed steel ρ_{ps} results in very modest decrease in prestress loss, as can be seen by comparing Fig. 5.2(a) and (b).
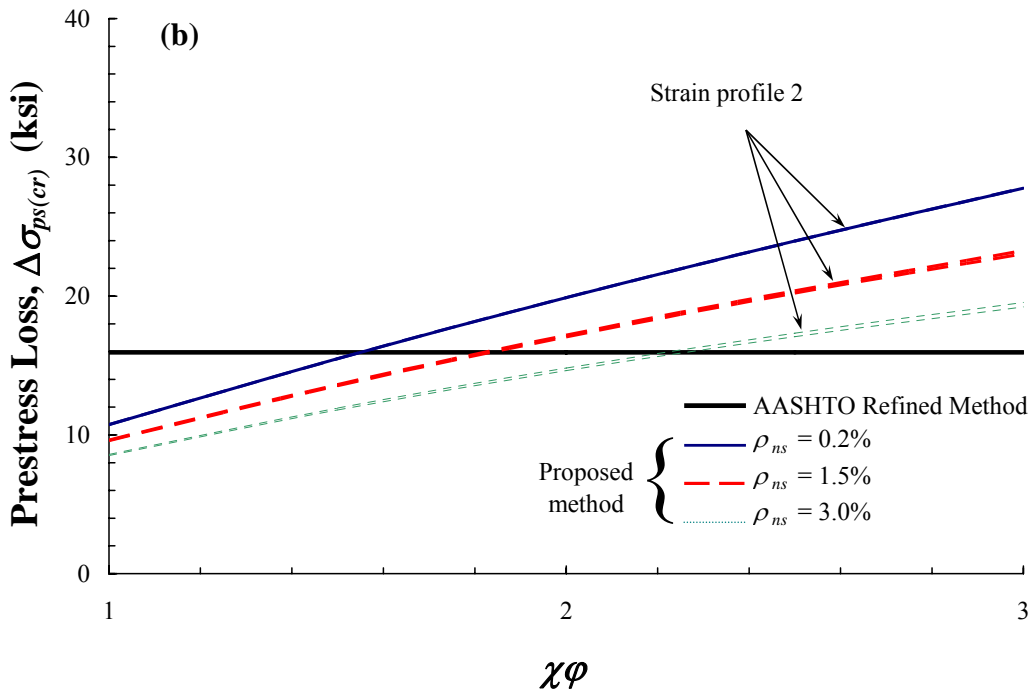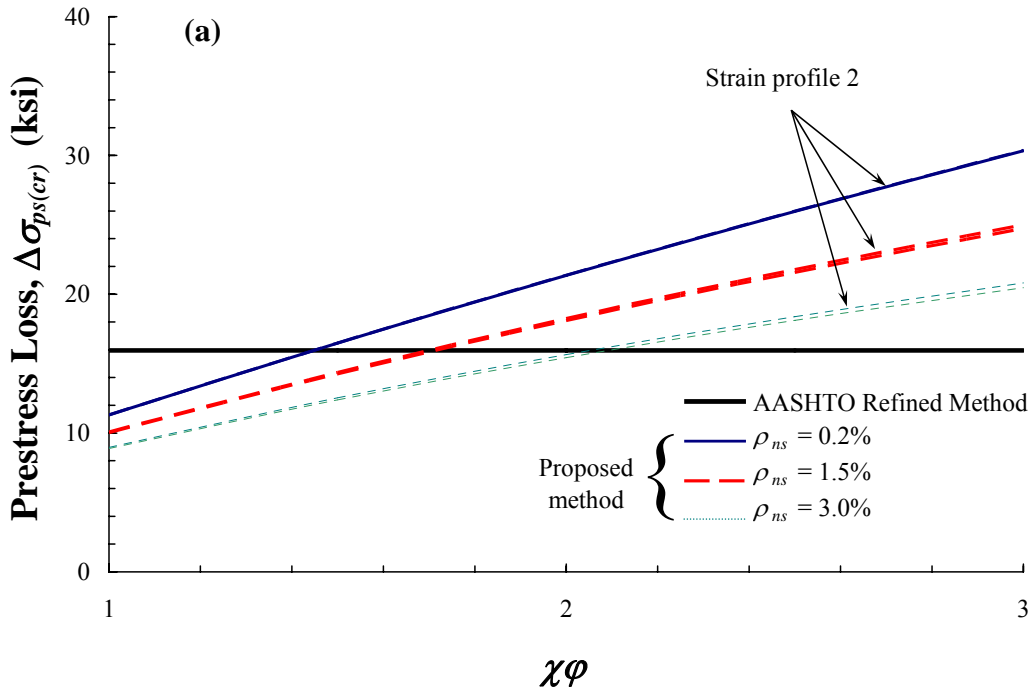
Fig. 5.2 Comparison between proposed method and AASHTO-LRFD refined method for long-term prestress losses due to creep: (a) $\rho_{ps} = 0.8\%$; and (b) $\rho_{ps} = 1.2\%$.

24

The current AASHTO-LRFD equation (Eq. 3.2) for prestress loss due to shrinkage is only a function of the relative humidity, RH. Although relative humidity is one of the major factors that affect concrete shrinkage, it is not the sole factor (see Section 2.1). As mentioned in Section 4.6, post-tensioned bridges in California have a V/S ratio that ranges from 5 to 7 in. For moist-cured concrete at a relative humidity of 40%, the AASHTO-LRFD shrinkage model predicts an ultimate shrinkage strains of 500×10^{-6} and 330×10^{-6}, respectively, for bridge cross sections having $V/S = 5$ in. and 7 in. (Note that this difference margin could even be higher when comparing with pretensioned bridges, which normally have V/S ratio of 3 in. to 4 in.) In other words, the AASHTO equation predicts the same amount of shrinkage losses for two bridge cross sections subjected to different shrinkage strains. As shown in Eq. 5.2, the prestress loss due to shrinkage $\Delta\sigma_{ps(sh)}$ varies directly with the shrinkage strain ε_{cs}. It is evident that an equation for prestress loss due to shrinkage should be a function of shrinkage strain ε_{cs} rather than relative humidity RH.

Figure 5.3 compares the predictions of the proposed method with the current AASHTO equation (Eq. 3.2) for prestress losses due to shrinkage. In applying Eq. 5.2, k_A and k_h depend upon $\chi\varphi$. Given the narrow range of variation of φ according to the AASHTO creep model (see Fig. 5.2), a constant value of 1.5 was assumed for $\chi\varphi$. This corresponds to a creep coefficient φ of 1.9, which is an approximate mean value for creep coefficients predicted by AASHTO. The shrinkage strain ε_{cs} in Eq. 5.2 was taken according the AASHTO shrinkage model. The apparent kink in the proposed method curves at $RH = 80\%$ is due to the fact that AASHTO shrinkage model uses different coefficients for RH higher than 80%. For most of the range studied for RH, the AASHTO prediction underestimates shrinkage losses for members with $V/S = 5$ in., whereas changes from overestimating to underestimating the losses as RH increases for members with $V/S = 7$ in. The increase in the ratio of non-prestressed steel ρ_{ns} reduces the amount of prestress loss, but this reduction is more pronounced in the case of $V/S = 5$ in. As in the case with losses due to creep, the effect of prestressed steel ratio ρ_{ps} is insignificant.
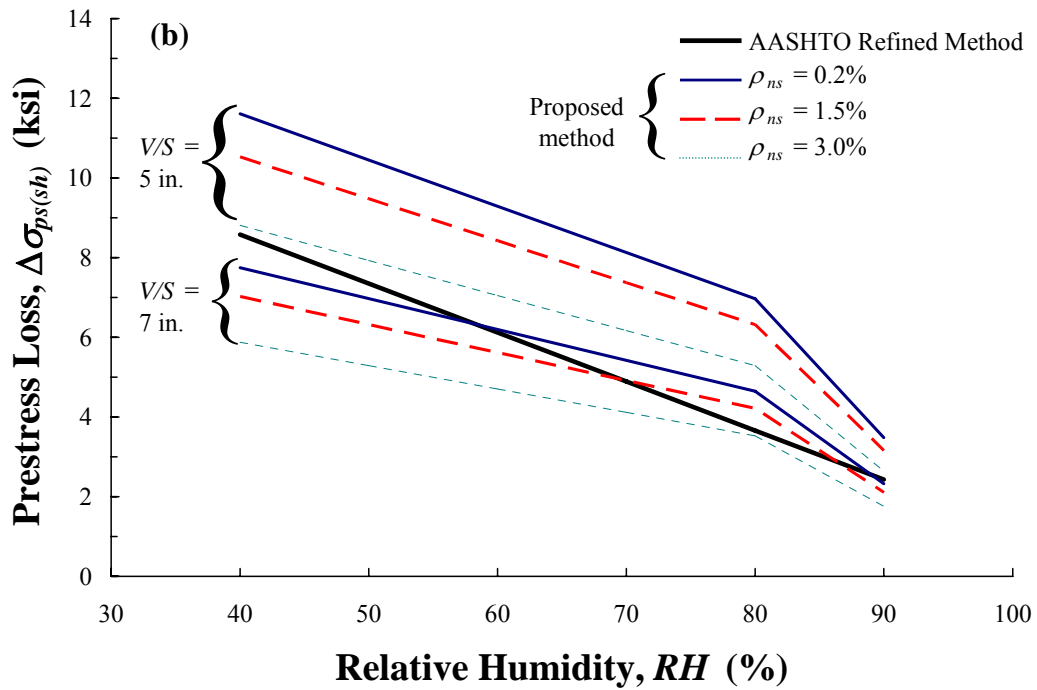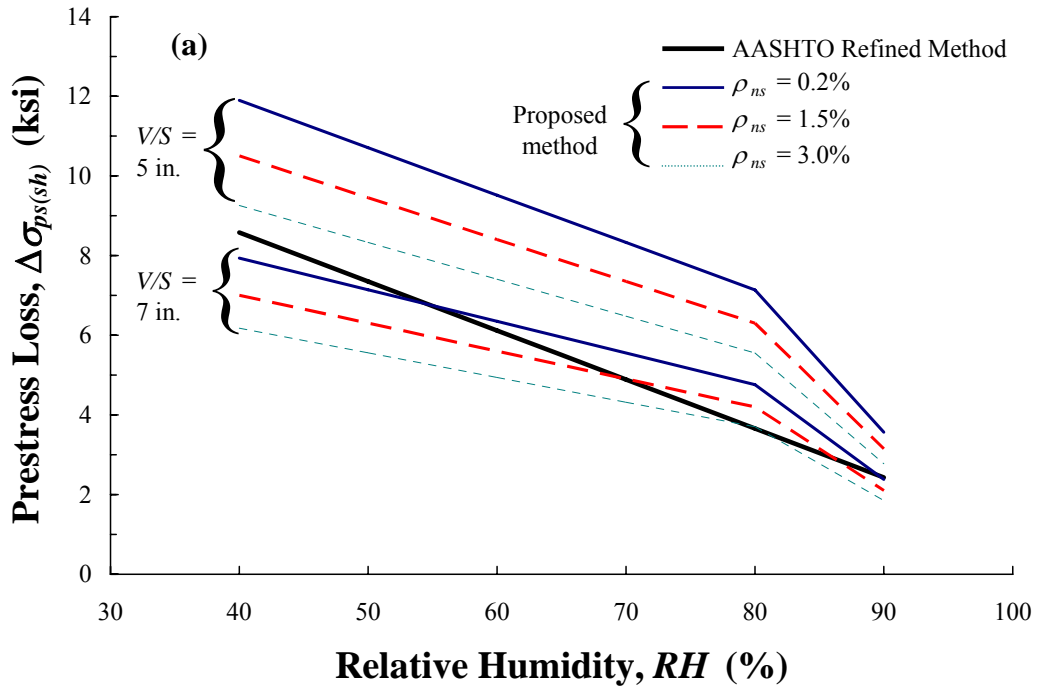
Fig. 5.3 Comparison between proposed method and AASHTO-LRFD refined method for long-term prestress losses due to shrinkage: (a) $\rho_{ps} = 0.8\%$; and (b) $\rho_{ps} = 1.2\%$.

The total long-term prestress losses are those due to the combined effects of creep, shrinkage of concrete and relaxation of prestressing steel. To evaluate the total long-term prestress losses using the proposed method, Eq. 4.18 (or adding up Eqs. 5.1 and 5.2) was used for the prestress losses due to creep and shrinkage; Eq. 4.22 was used for the prestress loss due to steel relaxation. The creep coefficient φ was varied to give $\chi\varphi$ values between 1 and 3 and the concrete shrinkage ε_{sc} was assumed a constant value 500 $\times$ 10^{-6}. Equations 3.1, 3.2, and 3.3 were used, respectively, to calculate the prestress losses due to creep, shrinkage, and relaxation in the AASHTO- LRFD refined method. In Eq. 3.3, the terms $\Delta\sigma_{ps(fr)}$ and $\Delta\sigma_{ps(es)}$ (prestress losses due to friction and elastic shortening, respectively) were not taken into account because: (1) $\Delta\sigma_{ps(fr)}$ depends on the profile of prestressing tendons and the duct material, factors that are not considered in the present study and are believed to have little or no impact on long-term prestress losses; and (2) There are no elastic losses ($\Delta\sigma_{ps(es)}$ = 0) for post-tensioned girders with one layer of prestressing, as assumed in the present study. In the AASHTO-LRFD approximate method (Eqs. 3.4 and 3.5), the partial prestress ratio *PPR* (Eq. 3.6) was calculated assuming yield strength of prestressing steel f_{py} = 243 ksi (1675 MPa) and yield strength of non-prestressed steel f_y = 58 ksi (400 MPa).

The AASHTO-LRFD refined and approximate methods are compared with the proposed method in Fig. 5.4(a) and (b). Regardless the ratio of non-prestressed steel ρ_{ns}, the average and upper bound approximate methods consistently underestimate the total prestress losses. The predictions of the AASHTO refined method change from underestimating to overestimating the total prestress losses as the ratio $\chi\varphi$ increases.

The effect of the shape of strain profile at time of post-tensioning (Fig. 5.2) and prestresed steel ratio ρ_{ps} (Fig. 5.2 through 5.4) are shown to be insignificant. Therefore, these variables will be excluded in further comparisons with design specifications in this section.
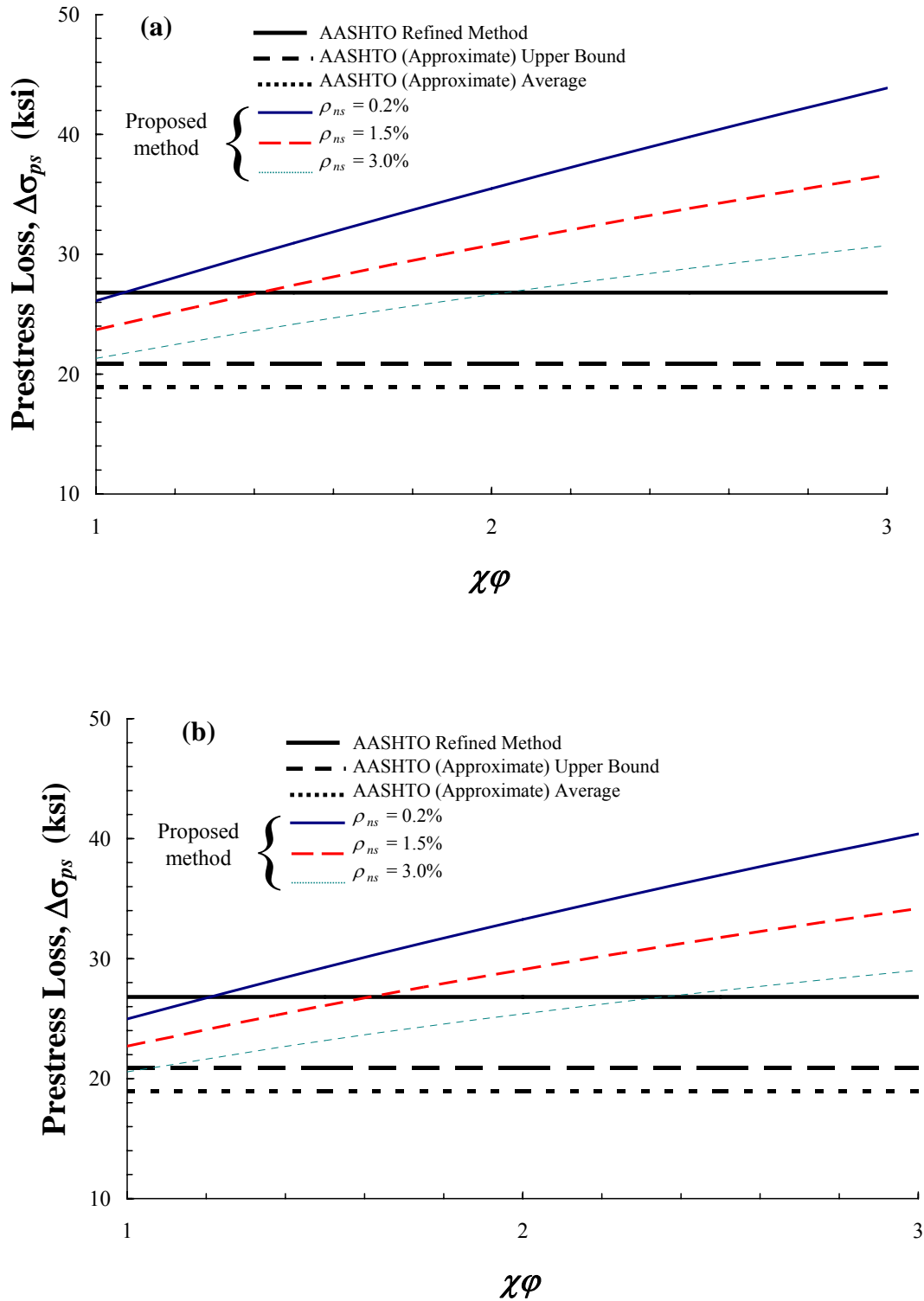
Fig. 5.4 Comparison between proposed method and AASHTO-LRFD refined and approximate methods for total prestress losses: (a) $\rho_{ps} = 0.8\%$; and (b) $\rho_{ps} = 1.2\%$.

5.2 CEB-FIP Model Code

The CEB-FIP predictions for long-term prestress losses due to the individual effects of creep and shrinkage can be given by Eqs. 5.4 and 5.5, respectively, considering only their respective terms in the numerator of Eq. 3.7:

$$\Delta\sigma_{ps(cr)} = \frac{\alpha_{ps}\varphi(t,t_0)f_{cgp}}{1+\alpha_{ps}\dfrac{A_{ps}}{A_c}\left(1+\dfrac{A_c y_{ps}^2}{I_c}\right)(1+\chi\varphi(t,t_0))} \tag{5.4}$$

$$\Delta\sigma_{ps(sh)} = \frac{E_{ps}\varepsilon_{cs}}{1+\alpha_{ps}\dfrac{A_{ps}}{A_c}\left(1+\dfrac{A_c y_{ps}^2}{I_c}\right)(1+\chi\varphi(t,t_0))} \tag{5.5}$$

The CEB-FIP MC predictions for creep losses (Eq. 5.4) are evaluated against the results of the proposed method (Eq. 5.1) in Fig. 5.5. As shown in the figure, the CEB-FIP overestimates the prestress losses since it does not take the effect of non-prestressed steel into account. As the non-prestressed steel ratio ρ_{ns} increases, the difference between the proposed method and the CEB-FIP becomes greater, as shown by the reduced slopes of the prediction curves of the proposed method compared with the CEB-FIP curves. On the other hand, the difference between the two methods increases with the increase in the creep coefficient φ.

A comparison between the proposed method (Eq. 5.2) and the CEB-FIP MC method (Eq. 5.5) for prestress losses due to shrinkage strain of 500×10^{-6} is shown in Fig. 5.6. Since both equations are linear functions in shrinkage, the conclusions outlined here is valid for any value of shrinkage strain. As expected, creep alleviates shrinkage effects and therefore shrinkage losses decrease with the increase in φ. The total prestress losses using the CEB-FIP method (Eq. 3.7) and the proposed method (Eq. 4.18 plus Eq. 4.22) are compared in Fig. 5.7. The concrete shrinkage ε_{cs} was assumed 500×10^{-6}. The general trend of the curves in Fig. 5.7 is quite similar to those in Fig. 5.5. The CEB-FIP consistently overestimates the total prestress losses, with increasing divergence from the proposed method with the increase in φ and ρ_{ns} values.
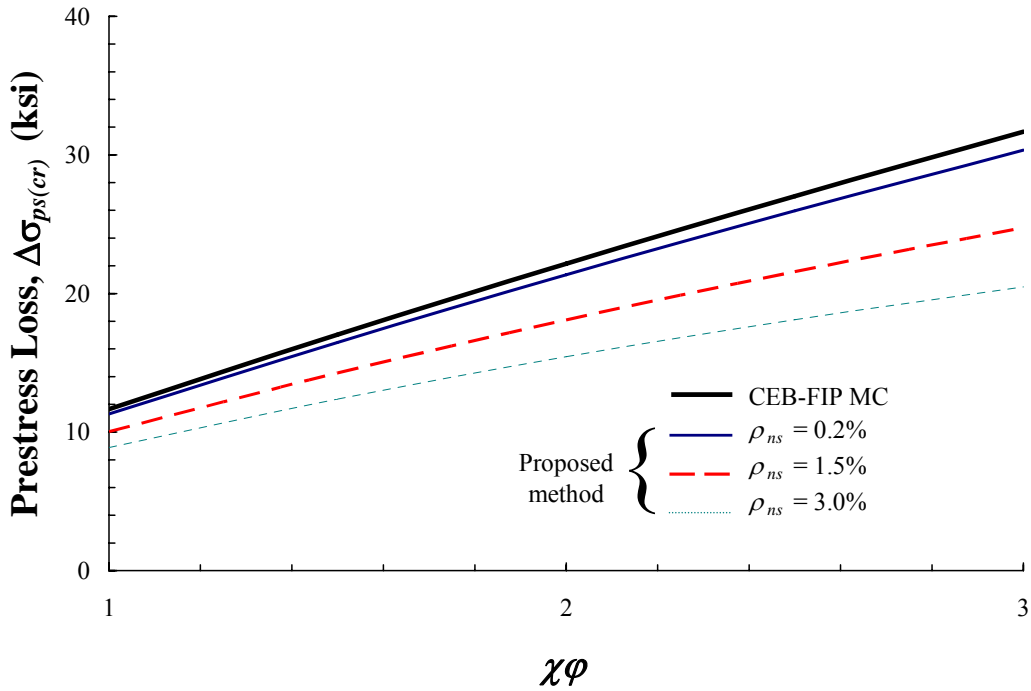
Fig. 5.5 Comparison between proposed method and CEB-FIP method for long-term prestress losses due to creep ($\rho_{ps} = 0.8\%$).
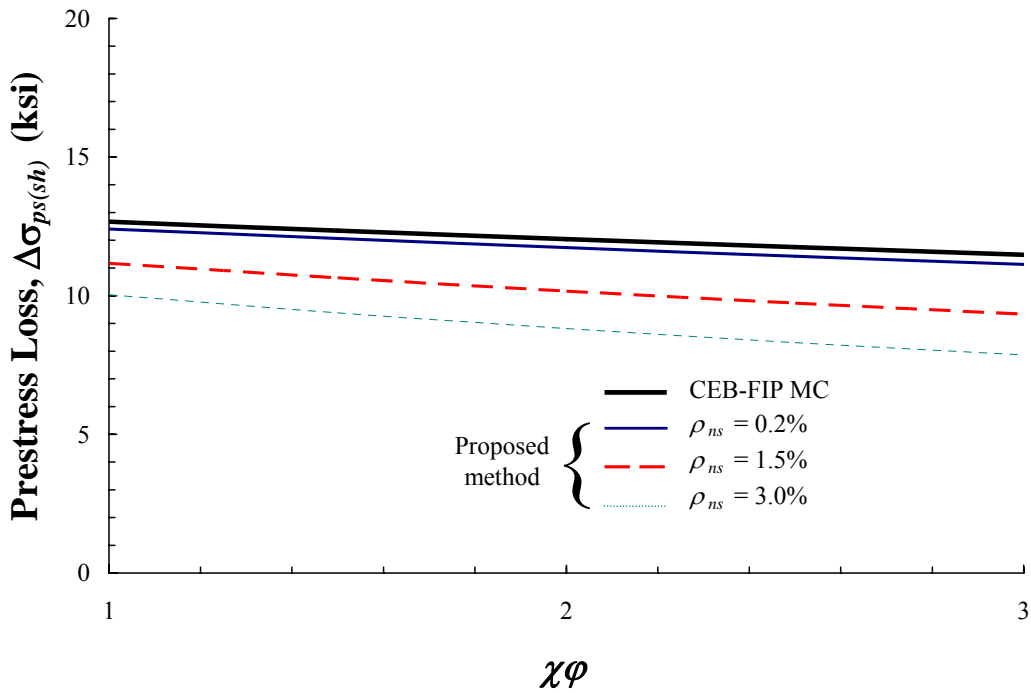

Fig. 5.6 Comparison between proposed method and CEB-FIP method for long-term prestress losses due to shrinkage ($\rho_{ps} = 0.8\%$).

Fig. 5.7 Comparison between proposed method and CEB-FIP method for total long-term prestress losses ($\rho_{ps} = 0.8\%$).

5.3 Canadian Highway Bridge Design Code (CHBDC)

The comparisons between the CHBDC and the proposed method with will be performed with respect to the relative humidity *RH* since it is the main variable in the CHBDC equations (Eq. 3.8 through 3.10). For each value of *RH*, the creep and shrinkage coefficients (to be used in the proposed method) were calculated using the empirical models of the CHBDC and assuming a *V/S* ratio of 5 in. It should be noted that an increase in *RH* essentially reduces the creep and shrinkage values. The prestress losses due to creep according to both methods are shown in Fig. 5.8. The CHBDC equation considerably underestimates prestress losses due to creep for all ratios of non-prestressed steel ρ_{ns}; the difference decreases with the increase in relative humidity *RH*.

Figure 5.9 shows the CHBDC and the proposed method predictions for shrinkage losses. In case of $\rho_{ps} = 0.2\%$, the CHBDC equation compares very well with the proposed

method. For ρ_{ns} = 1.5 and 3.0%, the CHBDC equation underestimates the shrinkage losses for *RH* values less than 70%; for higher values of *RH*, the CHBDC predictions compare well with the proposed method for all values of ρ_{ns}.

The total prestress losses using the proposed method (summation of Eq. 4.18 and 4.22) and CHBDC method (summation of Eq. 3.8 through 3.10) are compared in Fig. 5.10. In Eq. 3.10, f_{pu} was taken 270 ksi and the ratio of steel stress at transfer to ultimate strength σ_{p0}/f_{pu} was assumed 0.7. The CHBDC predictions significantly underestimate the total losses, except for sections with ρ_{ns} = 0.2% and RH greater than 75%. Similar to the observations made for creep losses, the difference between the two methods decreases with increasing *RH* values.

Fig. 5.8 Comparison between proposed method and CHBDC method for long-term prestress losses due to creep (ρ_{ps} = 0.8%).

Fig. 5.9 Comparison between proposed method and CHBDC method for long-term prestress losses due to shrinkage (ρ_{ps} = 0.8%).
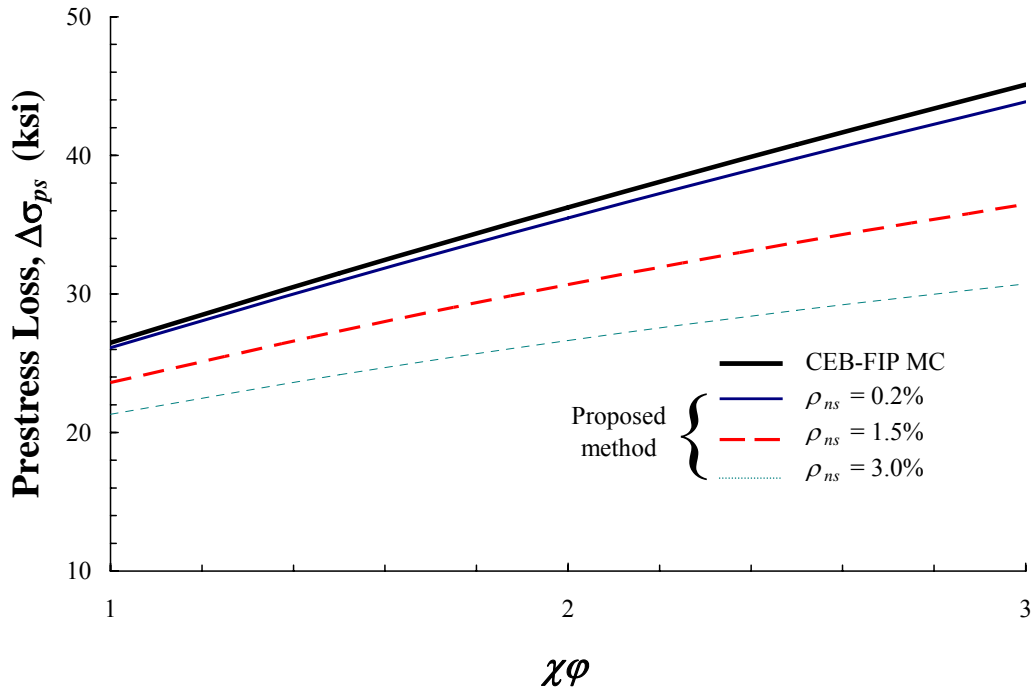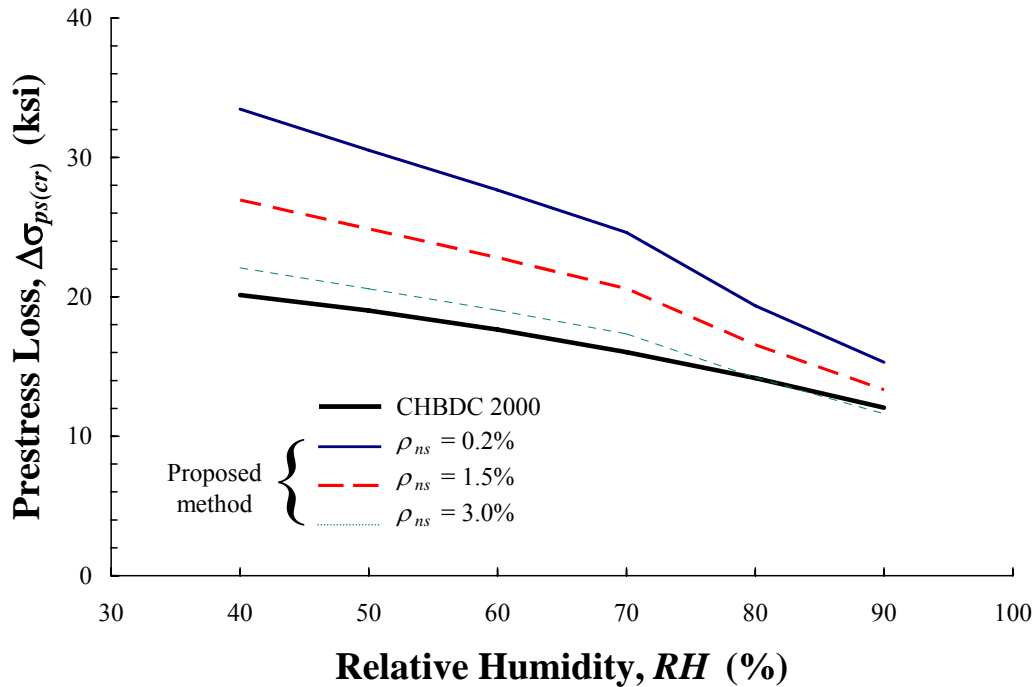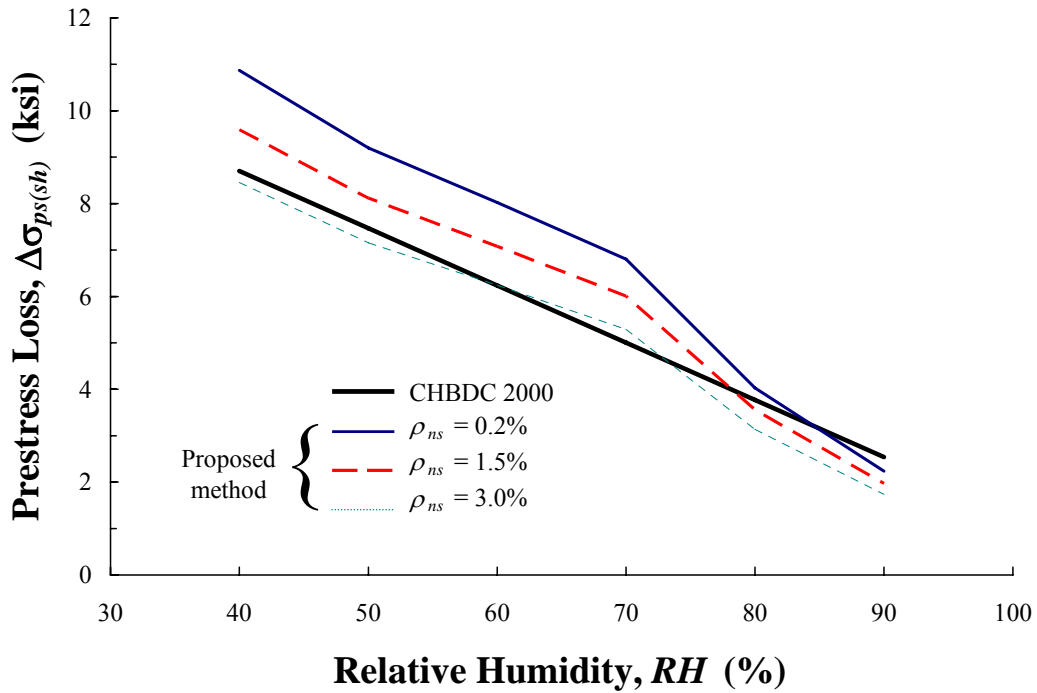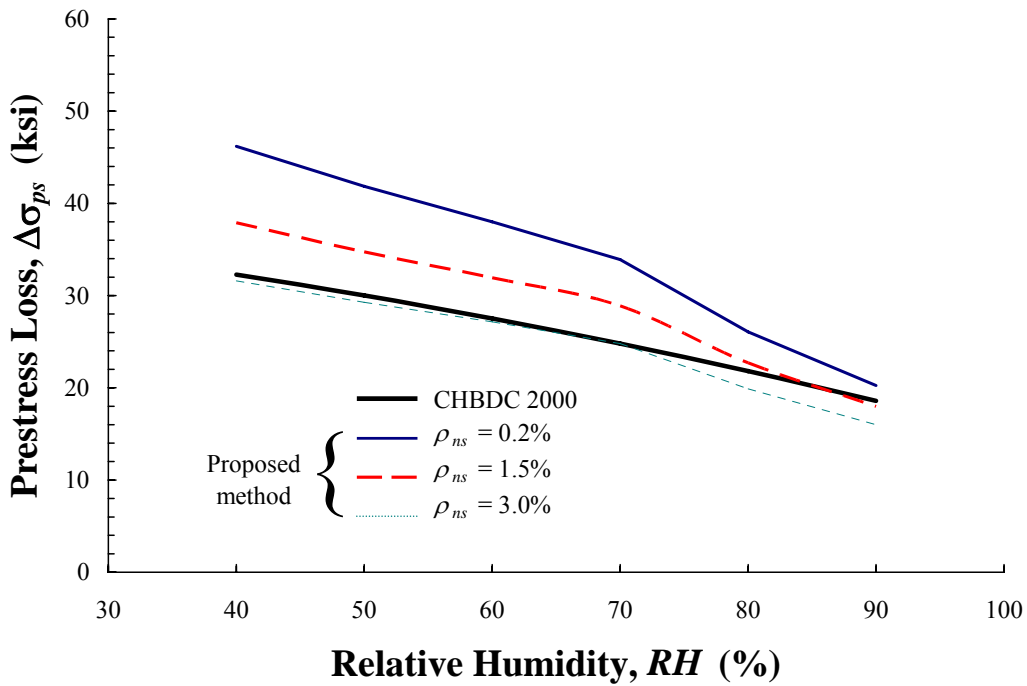

Fig. 5.10 Comparison between proposed method and CHBDC method for total long-term prestress losses (ρ_{ps} = 0.8%).

6. Examples

To further illustrate the use of the proposed method, two examples of cast-in-place post-tensioned bridges currently under construction in San Diego County will be analyzed for long-term prestress losses; the results from the proposed model will be compared with the current specifications of bridge codes. Since the construction drawings for these bridges were produced in SI units, the input data and results in this section, unlike the rest of the report, will be given in SI units only. The following parameters are assumed in the analysis of both bridges: $\varphi = 2.5$; $\chi = 0.8$; $\varepsilon_{cs} = -500 \times 10^{-6}$; $E_c(t_0) = 22.5$ GPa; $E_{ps} = 195$ GPa; $E_{ns} = 200$ GPa. To account for immediate losses, the curvature friction coefficient μ and anchor set are assumed 0.2 and 10 mm, respectively. Since only one layer of prestressing is assumed, there are no immediate losses due to elastic shortening.

6.1 Lake Hodges Bridge

Fig. 6.1 shows a half elevation and a half cross section of the Lake Hodges Bridge. Sections A to E shown in Fig. 6.1(a) are analyzed. The concrete dimensions of the bridge at the analyzed sections are shown in Fig. 6.1(b) and Table 6.1. The non-prestressed steel ratios at top and bottom slabs, ρ_{ns1} and ρ_{ns2}, respectively, and the prestressed steel ratio ρ_{ps}, are listed in Table 6.2. The variation of the prestressing force P after transfer, as a result of immediate losses, and its location d_{ps} are also given in Table 6.2; post-tensioning is performed from both ends.

Fig. 6.1(a)

34
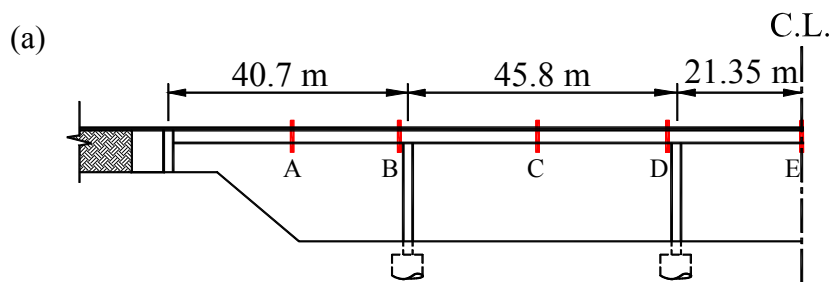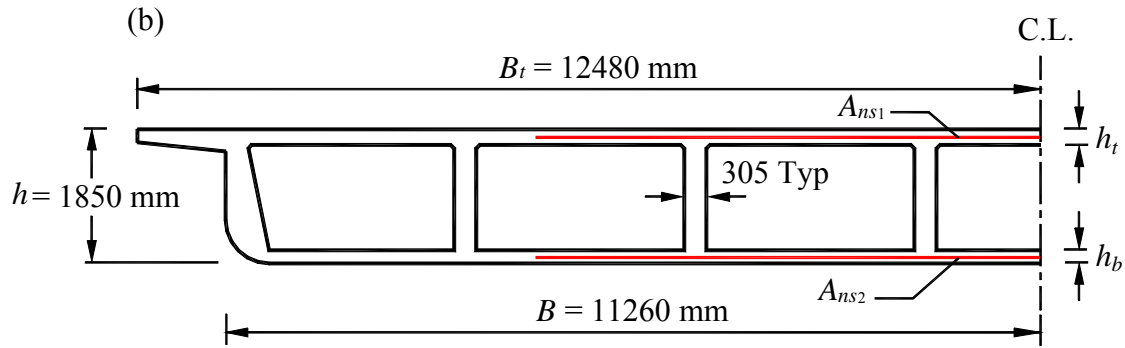
Fig. 6.1 Lake Hodges Bridge: (a) Half elevation; and (b) Half cross section.

Table 6.1 Lake Hodges Bridge: Concrete Dimensions

Section	h_t	h_b	B_t/B	$\Sigma B_w/B$	h_t/h	h_b/h
A	215	180	1.11	0.12	0.12	0.1
B	215	305	1.11	0.12	0.12	0.16
C	215	180	1.11	0.12	0.12	0.1
D	215	305	1.11	0.12	0.12	0.16
E	215	180	1.11	0.12	0.12	0.1

Table 6.2 Lake Hodges Bridge: Reinforcement and Prestressing

Section	A_{ns1} (mm²)	ρ_{ns1} (%)	A_{ns2} (mm²)	ρ_{ns2} (%)	A_{ps} (mm²)	ρ_{ps} (%)	d_{ps} (mm)	d_{ps}/h	P (kN)
A	32290	0.6	22060	0.54	42280	1.06	1510	0.82	55576
B	67410	1.25	46111	0.67	42280	1.16	355	0.19	55732
C	32290	0.6	22060	0.54	42280	1.06	1510	0.82	53472
D	67410	1.25	46111	0.67	42280	1.16	355	0.19	51303
E	32290	0.6	22060	0.54	42280	1.06	1510	0.82	49079

The coefficients k_A, k_I, and k_h (Eq. 4.15) are evaluated for each section and listed in Table 6.3. The computer program CPF[13] is used to analyze the bridge due to its own weight and prestressing. The output results from the program were used to determine the strain at the centroid of net concrete section $\varepsilon_O(t_0)$ and the slope of the strain diagram $\psi(t_0)$. The prestress loss due to creep and shrinkage $\Delta\sigma_{ps}$ is calculated using Eqs. 4.16 and 4.18. The prestress loss due to continuity $\Delta\sigma_{ps(cont)}$ is evaluated using Eqs. B.17 through B.23. As can be seen from Table 6.3, $\Delta\sigma_{ps(cont)}$ is a very small amount compared to $\Delta\sigma_{ps}$. The total pestress loss $\Delta\sigma_{ps(total)}$ is given is the right column of the table.

The prestress loss for Lake Hodges Bridge using various code predictions are listed and compared to those of the proposed method in Table 6.4. While the AASHTO approximate method predictions are close to those of the proposed method, the AASHTO detailed method underestimates the total losses by an average of 24%. On the other hand, the CEB-FIP and the CHBDC predictions are, respectively, 13% higher and 11% less than the predictions of the proposed method. It should be noted that the comparison results in Table 6.4 are intended only to this particular bridge along with the creep and shrinkage values considered and should not be taken as a general conclusion. Even without changing the creep and shrinkage values, these ratios could change with changing the bridge cross-section, as will be seen in the next comparison.

Table 6.3 Lake Hodges Bridge: Analysis results

Section	k_A	k_I	k_h	$\varepsilon_O(t_0)$ (x 10^{-6})	$\psi(t_0)$ (x 10^{-6}/m)	$\Delta\sigma_{ps}$ (MPa)	$\Delta\sigma_{ps(cont)}$ (MPa)	$\Delta\sigma_{ps(total)}$ (MPa)
A	0.84	0.83	0.13	-180	34	139	1	140
B	0.79	0.77	-0.15	-149	-65	112	-1	111
C	0.84	0.83	0.13	-173	14	142	0	142
D	0.79	0.77	-0.15	-137	-37	114	1	115
E	0.84	0.83	0.13	-159	-6	142	-2	140

Table 6.4 Lake Hodges Bridge: Comparison with design specifications

Section	AASHTO Approximate		AASHTO Detailed		CEB-FIP		CHBDC	
	$\Delta\sigma_{ps}$	Ratio*	$\Delta\sigma_{ps}$	Ratio*	$\Delta\sigma_{ps}$	Ratio*	$\Delta\sigma_{ps}$	Ratio*
A	128	0.91	102	0.73	151	1.08	121	0.86
B	123	1.11	89	0.80	134	1.21	102	0.92
C	128	0.90	103	0.73	154	1.09	123	0.87
D	123	1.08	90	0.79	136	1.19	104	0.91
E	128	0.90	103	0.73	154	1.08	123	0.87
Average		0.98		0.76		1.13		0.89

* Ratio of prestress loss using design specification to that of the proposed method.

6.2 Duenda Road Over crossing

Fig. 6.2 shows an elevation and a cross section of the Duenda Road Over crossing. Sections A to C shown in Fig. 6.2(a) are analyzed. The concrete dimensions of the bridge at the analyzed sections are shown in Fig. 6.1(b) and Table 6.5. Non-prestressed and prestressing steel data are given in Table 6.6. Post-tensioning is performed from the long-span end. The analysis results and comparisons with design specifications are reported in Tables 6.7 and 6.8, respectively. The reason for choosing this bridge for analysis is to determine whether a significant difference in the length of two adjacent spans in a continuous bridge could have any effect on the prestress losses due to continuity. As shown in Table 6.7, the continuity effect is quite insignificant and could be ignored. This could be explained by referring to Eq. 4.17, which shows that the prestress loss depends on the change in axial strain at the centroid of the net concrete section $\Delta\varepsilon_O$ and the change in curvature $\Delta\psi$. For most practical applications, the change in axial strain is the most dominant factor. The analysis for continuity effects only calculates the additional change in $\Delta\psi$. In addition, in the calculation of angular discontinuity ΔD_1 at one end of intermediate support (see for instance Eq. 4.25 for two spans) $(\Delta\psi)_A$ and $(\Delta\psi)_B$ are of

opposite signs therefore reduce ΔD_1, which in turn reduces the long-term change in continuity moment ΔF_1.
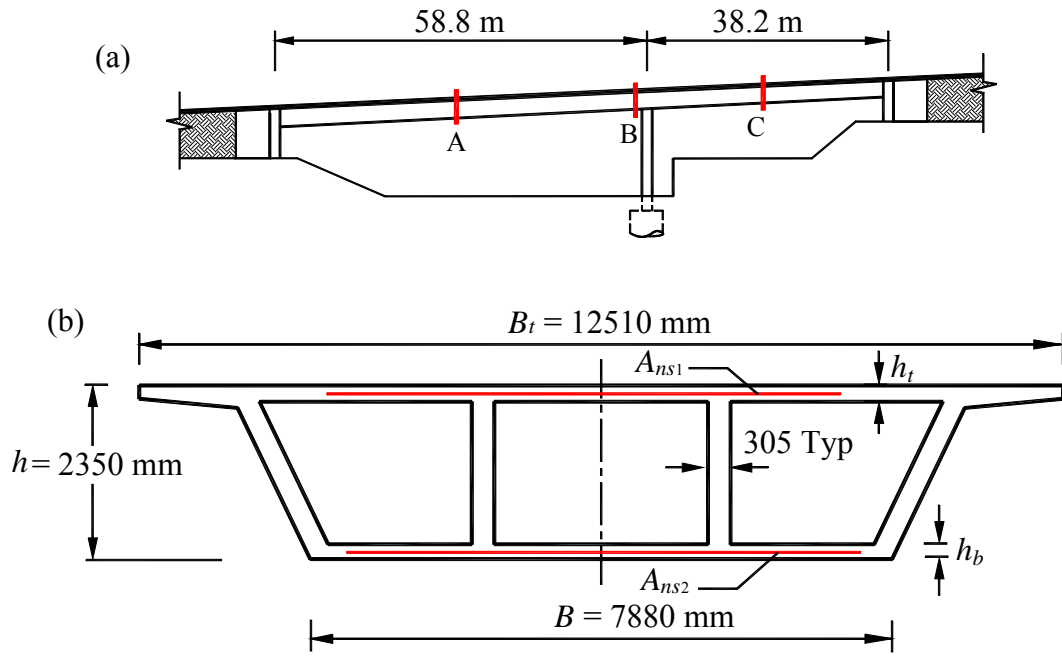

Fig. 6.2 Duenda Road Over crossing: (a) Elevation; and (b) Cross section.

Table 6.5 Duenda Road Over-crossing: Concrete Dimensions

Section	h_t	h_b	B_t/B	$\Sigma B_w/B$	h_t/h	h_b/h
A	220	185	1.51	0.16	0.09	0.08
B	220	305	1.51	0.16	0.09	0.13
C	220	255	1.51	0.16	0.09	0.11

Table 6.6 Duenda Road Over crossing: Reinforcement and Prestressing

Section	A_{ns1} (mm²)	ρ_{ns1} (%)	A_{ns2} (mm²)	ρ_{ns2} (%)	A_{ps} (mm²)	ρ_{ps} (%)	d_{ps} (mm)	d_{ps}/h	P (kN)
A	11148	0.43	10001	0.69	36000	1.19	1890	0.80	44788
B	27837	1.07	14910	0.57	36000	1.19	460	0.20	44411
C	24401	1.21	14910	0.74	36000	1.19	1145	0.49	43855

Table 6.7 Duenda Road Over crossing: Analysis results

Section	k_A	k_I	k_h	$\varepsilon_O(t_0)$ (x 10⁻⁶)	$\psi(t_0)$ (x 10⁻⁶ /m)	$\Delta\sigma_{ps}$ (MPa)	$\Delta\sigma_{ps(cont)}$ (MPa)	$\Delta\sigma_{ps(total)}$ (MPa)
A	0.81	0.80	0.27	-343	-45	162	1	163
B	0.78	0.79	-0.20	-122	-123	136	-2	134
C	0.78	0.83	-0.005	-335	63	175	0	175

Table 6.8 Duenda Road Over crossing: Comparison with design specifications

Section	AASHTO Approximate		AASHTO Detailed		CEB-FIP		CHBDC	
	$\Delta\sigma_{ps}$	Ratio*	$\Delta\sigma_{ps}$	Ratio*	$\Delta\sigma_{ps}$	Ratio*	$\Delta\sigma_{ps}$	Ratio*
A	129	0.79	129	0.79	173	1.06	160	0.98
B	129	0.96	107	0.80	154	1.15	129	0.96
C	129	0.74	130	0.74	199	1.14	162	0.93
Average		0.83		0.78		1.12		0.96

* Ratio of prestress loss using design specification to that of the proposed method.

7. Conclusions

Based on the analytical studies presented in the present section, the following conclusions can be made:

- The long-term behavior of concrete bridges is a rather involved procedure that depends on many parameters. The prediction of long-term prestress losses from equations that are function of only one or two parameters, as in the case of all the equations of bridge codes, cannot produce accurate results for all cases.

- Although relative humidity is one of the major factors that affect the shrinkage and creep strains, it is not the only one. Equations for prestress losses that are functions of only the relative humidity can lead to misleading results. It is recommended that the prediction equations be functions of the creep and shrinkage coefficients as determined from codes of practice.

- Accounting for the effect of non-prestressed steel is very essential to produce reliable results for prestressing losses. Neglecting this effect, as in the case of the CEB-FIP method, can greatly overestimate the prestress losses. Taking this effect into account in an empirical fashion, as in the case of the other prediction equations, can produce predictions that do not follow the actual trend of prestress losses.

- The AASHTO-LRFD upper bound approximate method is in fact a lower bound. The approximate average method lies outside the range of prestress loss predictions.

- The CHBDC gives reasonable and better predictions for prestress losses compared with the AASHTO-LRFD and CEB-FIP methods.

References

1. Trost, H., "Auswirkungen des Superpositionspringzips auf Kriech-und Relaxations-problems bei Beton und Apannbeton," *Beton und Stahlbetonbau,* V. 62, No. 10, 1967, pp. 230-238; No. 11, 1967, pp. 261-269 (in German).

2. Bazant, Z.P., "Prediction of Concrete Creep Effects Using Age-Adjusted Effective Modulus," *ACI Journal,* V. 69, No. 4, 1972, pp. 212-217.

3. Magura, D.D., Sozen, M.A., and Siess, C.P., "A Study of Stress Relaxation in Prestressing Reinforcements," *PCI Journal,* V. 9, No. 2, 1964, pp. 13-57.

4. Ghali, A., and Trevino, J., "Relaxation of Steel in Prestressed Concrete," *PCI Journal,* V. 30, No. 5, 1985, pp. 82-94.

5. American Association of State Highway and Transportation Officials, "AASHTO-LRFD Bridge Design Specifications," Third Edition, Washington, DC, 2004.

6. Comité Euro-International du Beton − Fédération Internationale de la Précontrainte, "Model Code for Concrete Structures," CEB-FIP MC 90, London, UK, 1993.

7. Canadian Highway Bridge Design Code, CAN/CSA-S6-00, Rexdale, Canada, 2000.

8. Ghali, A., Favre, R., and Elbadry, M.M., "Concrete Structures: Stresses and Deformations," Third Edition, Spon Press, London & New York, 2002, 584 pp.

9. ACI Committee 209, "Prediction of Creep, Shrinkage, and Temperature Effects in Concrete Structures," Committee Report 209R-92, American Concrete Institute, Detroit, MI, 1992, 47 pp.

10. http://www.ncdc.noaa.gov/oa/climate/online/ccd/avgrh.html

11. Tadros, M.K., Al-Omaishi, N., Serguirant, S.J., and Gallt, J.G., "Prestress Losses in Pretensioned High-Strength Concrete Bridge Girders," NCHRP Report 496, *Transportation Research Board,* Washington, DC, 2003, 63 pp.

12. Ghali, A., Neville, A.M., and Brown, T.G., "Structural Analysis: A Unified Classical and Matrix Approach," Fifth Edition, Spon Press, London &New York, 2004, 844 pp.

13. Elbadry, M.M., and Ghali, A., "User's Manual and Computer Program CPF: Cracked Plane Frames in Prestressed Concrete," *Research Report CE 85-2*, Department of Civil Engineering, University of Calagry, Calgary, Alberta, Canada, 1990, 82 pp.

Appendix A: Coefficients k_A, k_I and k_h

Figures A.1 to A.18 give the coefficients k_A, k_I and k_h included in Eq. 4.18 to calculate the long-term prestress loss $\Delta\sigma_{ps}$. The symbols in the following figures are defined below (see Fig. 4.3):

B_t and B = widths of top and bottom flanges, respectively;

h_t and h_b = depths of top and bottom flanges, respectively;

h = total depth of concrete section;

A_{ns1} and A_{ns2} = areas of non-prestressed steel in top and bottom flanges, respectively;

A_{ps} = area of prestressing steel;

$\Sigma B_w = B_{w1} + B_{w2} + ...$ = summation of web widths of the cross section;

$\rho_{ns1} = A_{ns1}/B_t\, h_t$ = ratio of non-prestressed steel in top flange;

$\rho_{ns2} = A_{ns2}/B\, h_b$ = ratio of non-prestressed steel in bottom flange; and

$\rho_{ps} = A_{ps}/h\, \Sigma B_w$ = ratio of prestressing steel with respect to web areas.

In the graphs below, the modulus of elasticity of prestressing steel E_{ps} and non-prestressed steel E_{ns} were assumed 27.5 ksi (190 GPa) and 29 ksi (200 GPa), respectively. The modulus of elasticity of concrete E_c at time of post-tensioning was assumed 3.6 ksi (25 GPa); the aging coefficient χ was assumed 0.8. Two cases of top and bottom thicknesses were assumed: Case 1 h_t/h = 0.05 and h_b/h = 0.05; and Case 2 h_t/h = 0.15 and h_b/h = 0.15. The following should be noted when using these graphs:

- The value of k_A is the same for sections with d_{ps} = 0.8h or 0.2h; therefore, no distinction was indicated on the graphs.
- The value of k_I is the same for sections with d_{ps} = 0.8h or 0.2h and having B_t/B = 1. For sections having B_t/B = 2, two curves (in dashed lines) are shown for k_I.

- The value of k_h for sections with $d_{ps} = 0.2h$ and having $B_t/B = 1$ is the same (but with opposite sign) for sections with $d_{ps} = 0.8h$. For sections having $B_t/B = 2$, two curves (in dashed lines) are shown for k_h.
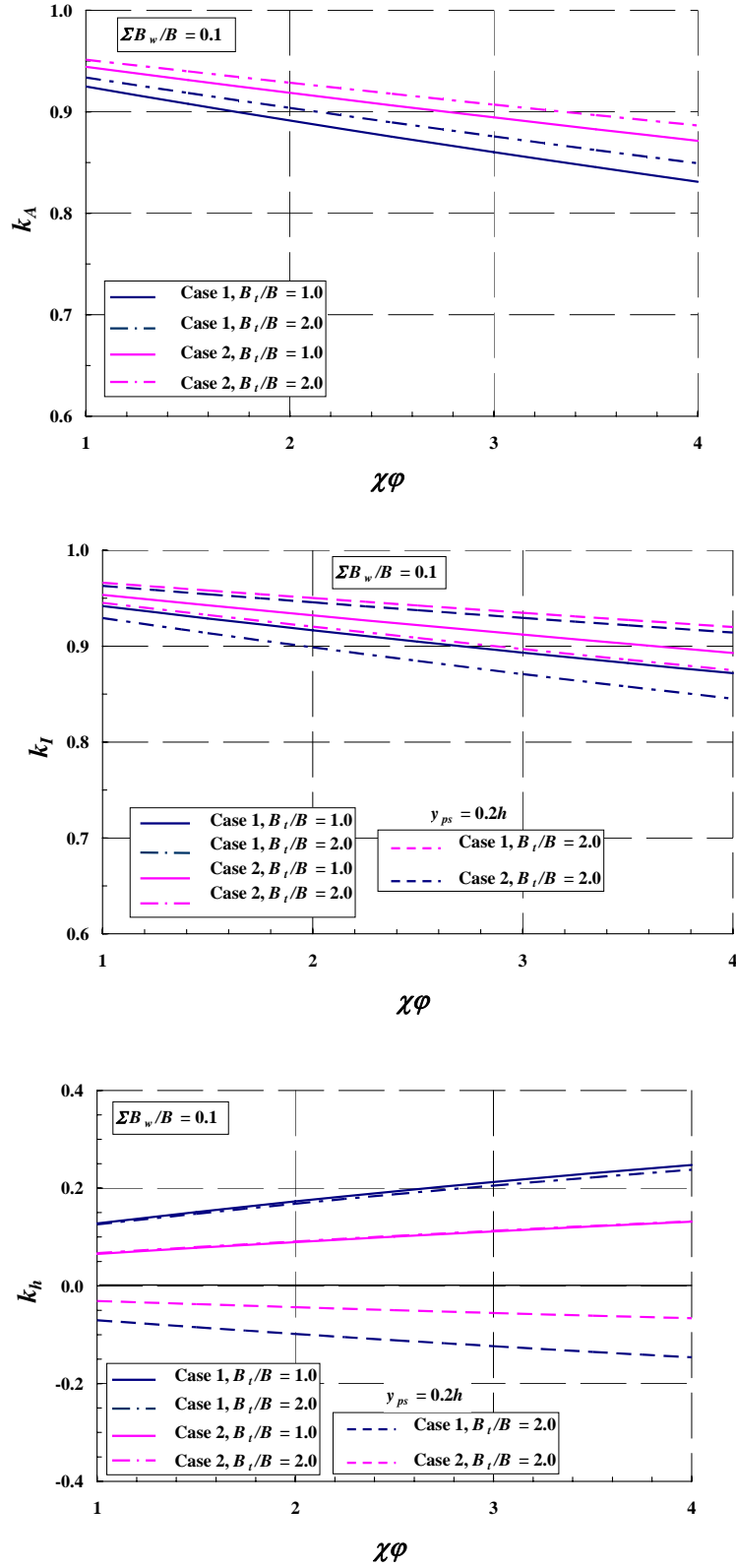
Fig. A.1 k_A, k_I and k_h for the case $\Sigma B_w/B = 0.1$, $\rho_{ns1} = \rho_{ns2} = 0.2\%$, $\rho_{ps} = 0.8\%$.
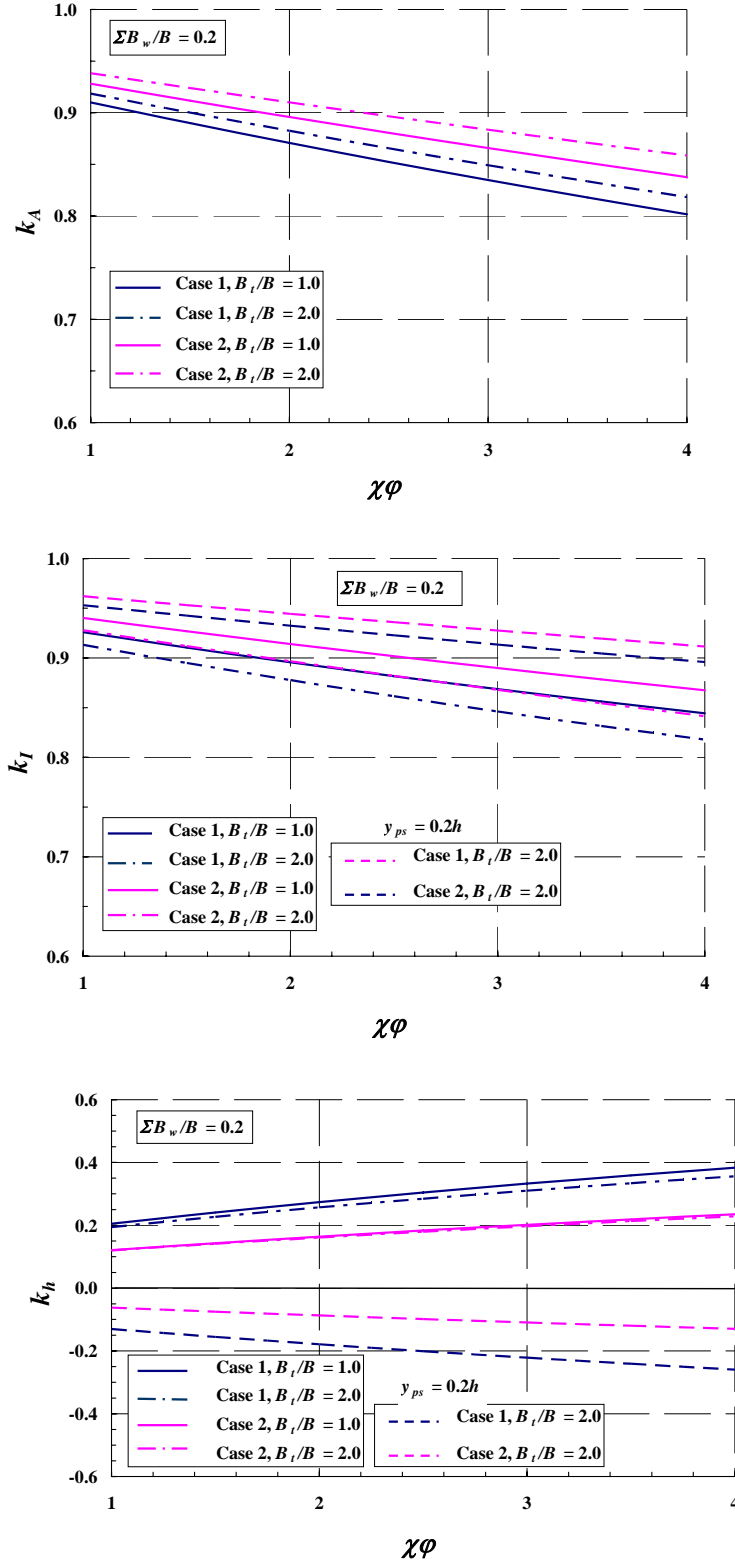
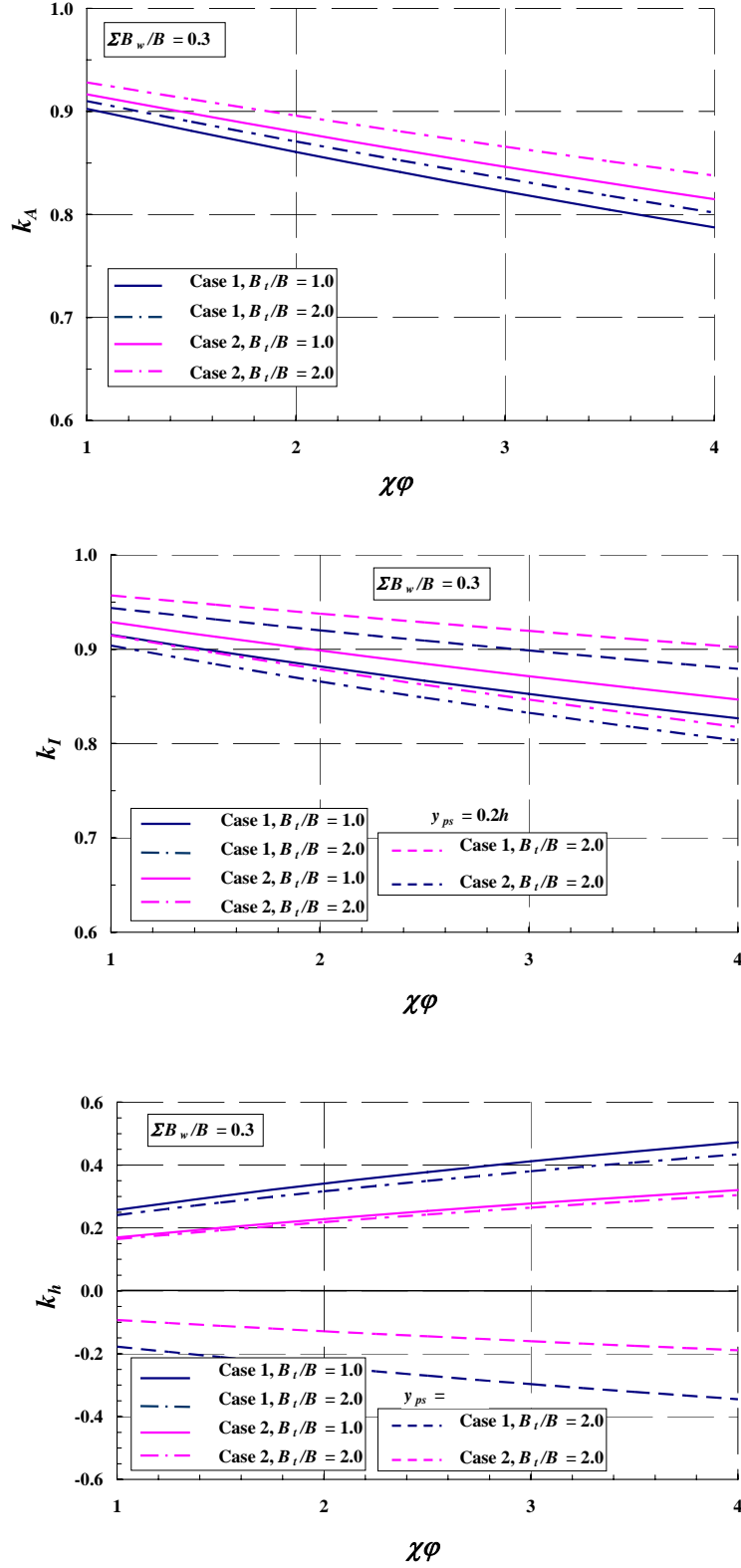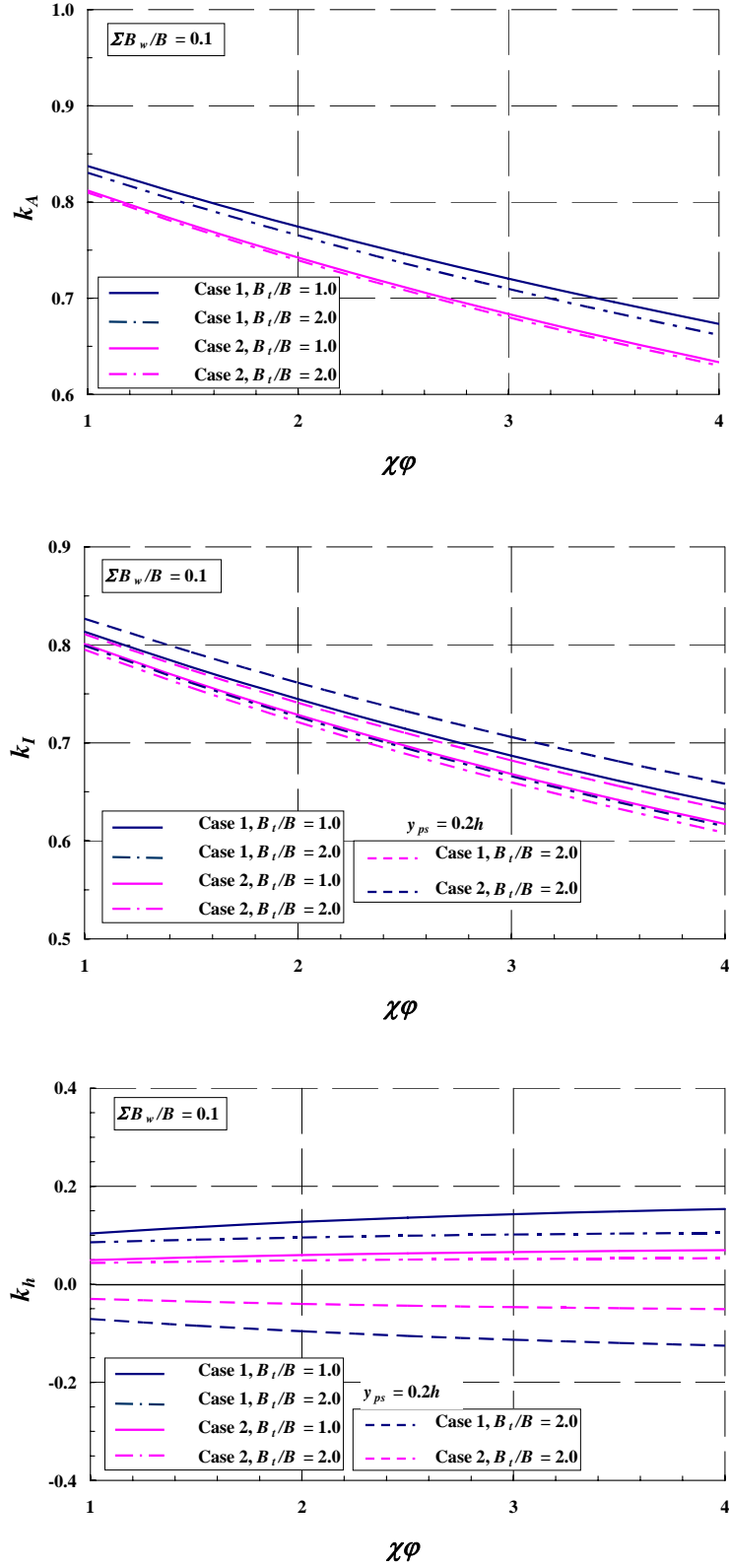Fig. A.2 k_A, k_I and k_h for the case $\Sigma B_w / B = 0.2$, $\rho_{ns1} = \rho_{ns2} = 0.2\%$, $\rho_{ps} = 0.8\%$.

Top chart (y-axis: k_A, x-axis: $\chi\varphi$)

$\Sigma B_w/B = 0.3$

Legend:
- Case 1, $B_t/B = 1.0$
- Case 1, $B_t/B = 2.0$
- Case 2, $B_t/B = 1.0$
- Case 2, $B_t/B = 2.0$

Middle chart (y-axis: k_I, x-axis: $\chi\varphi$)

$\Sigma B_w/B = 0.3$

Legend:
- Case 1, $B_t/B = 1.0$
- Case 1, $B_t/B = 2.0$
- Case 2, $B_t/B = 1.0$
- Case 2, $B_t/B = 2.0$

$y_{ps} = 0.2h$
- Case 1, $B_t/B = 2.0$
- Case 2, $B_t/B = 2.0$

Bottom chart (y-axis: k_h, x-axis: $\chi\varphi$)

$\Sigma B_w/B = 0.3$

Legend:
- Case 1, $B_t/B = 1.0$
- Case 1, $B_t/B = 2.0$
- Case 2, $B_t/B = 1.0$
- Case 2, $B_t/B = 2.0$

$y_{ps} =$
- Case 1, $B_t/B = 2.0$
- Case 2, $B_t/B = 2.0$

Fig. A.3 k_A, k_I and k_h for the case $\Sigma B_w/B = 0.3$, $\rho_{ns1} = \rho_{ns2} = 0.2\%$, $\rho_{ps} = 0.8\%$.
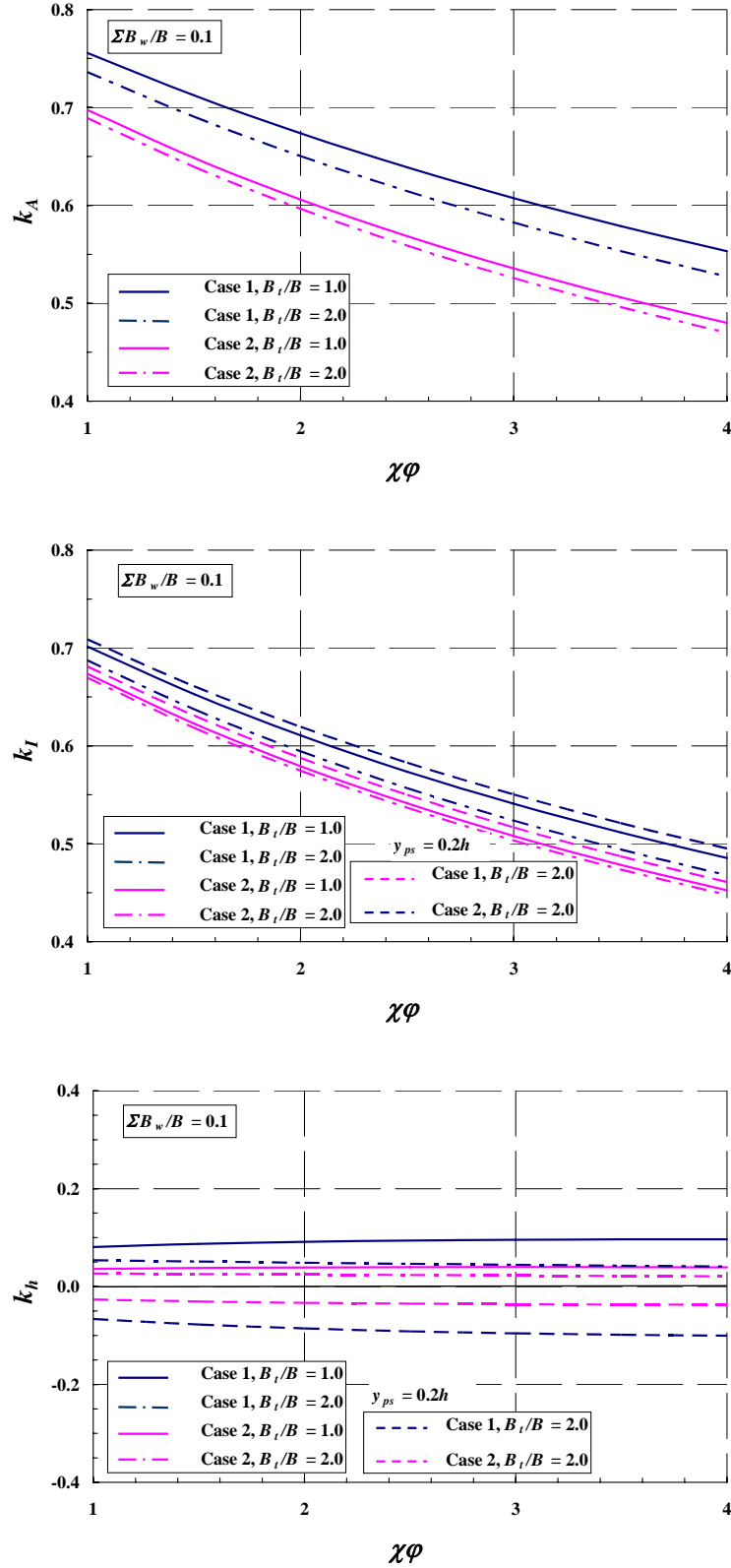
Fig. A.4 k_A, k_I and k_h for the case $\Sigma B_w/B = 0.1$, $\rho_{ns1} = \rho_{ns2} = 1.5\%$, $\rho_{ps} = 0.8\%$.
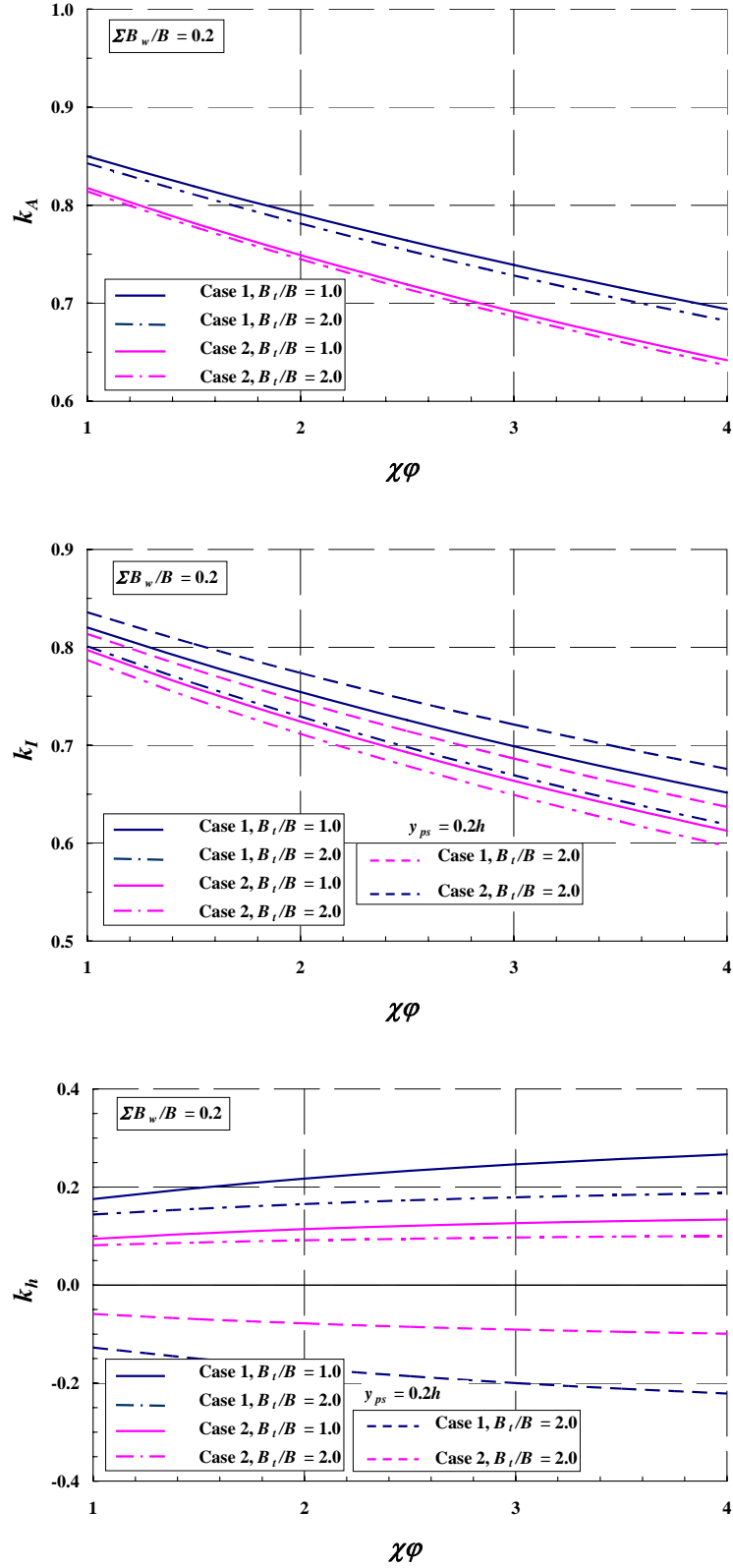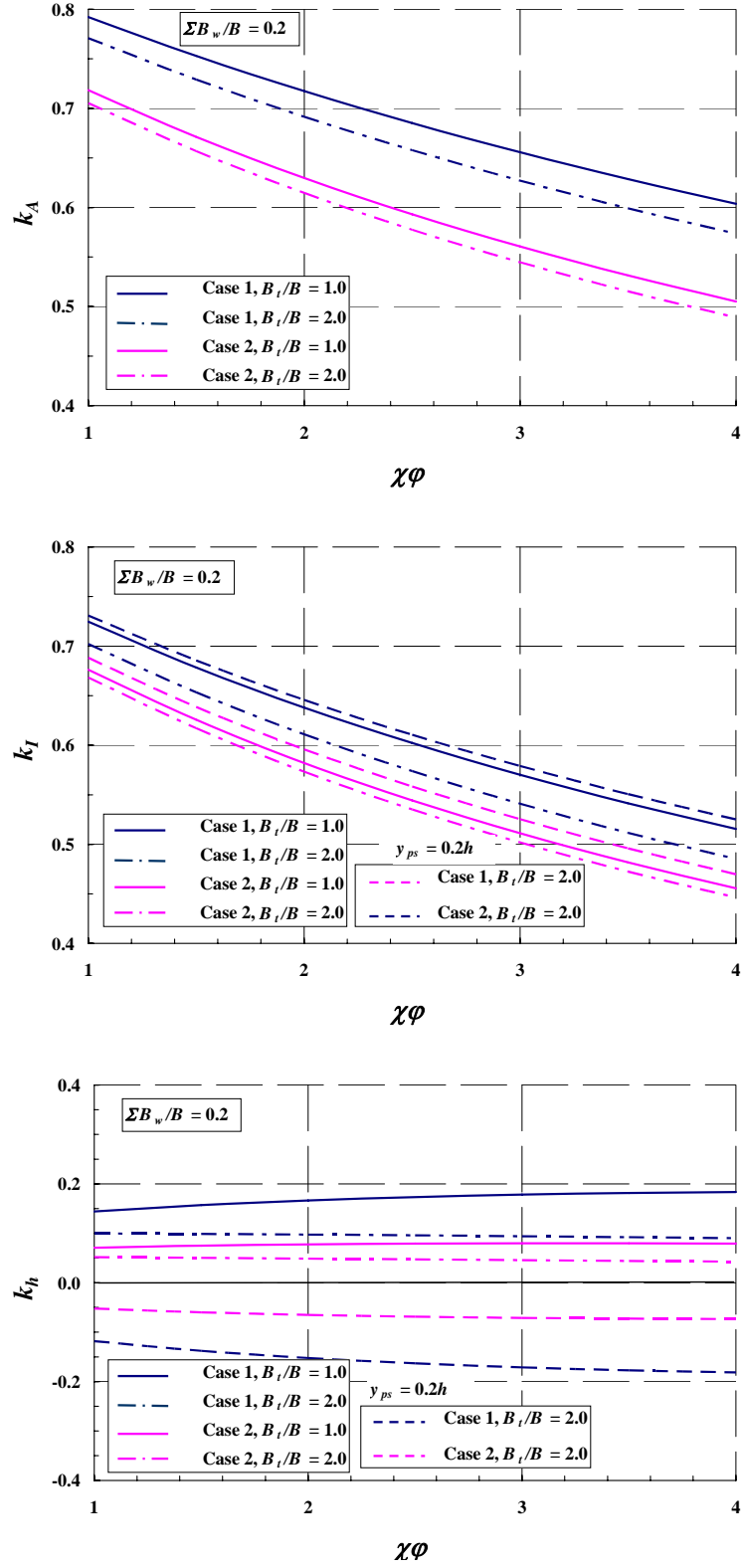
Fig. A.5 k_A, k_I and k_h for the case $\Sigma B_w/B = 0.2$, $\rho_{ns1} = \rho_{ns2} = 1.5\%$, $\rho_{ps} = 0.8\%$.
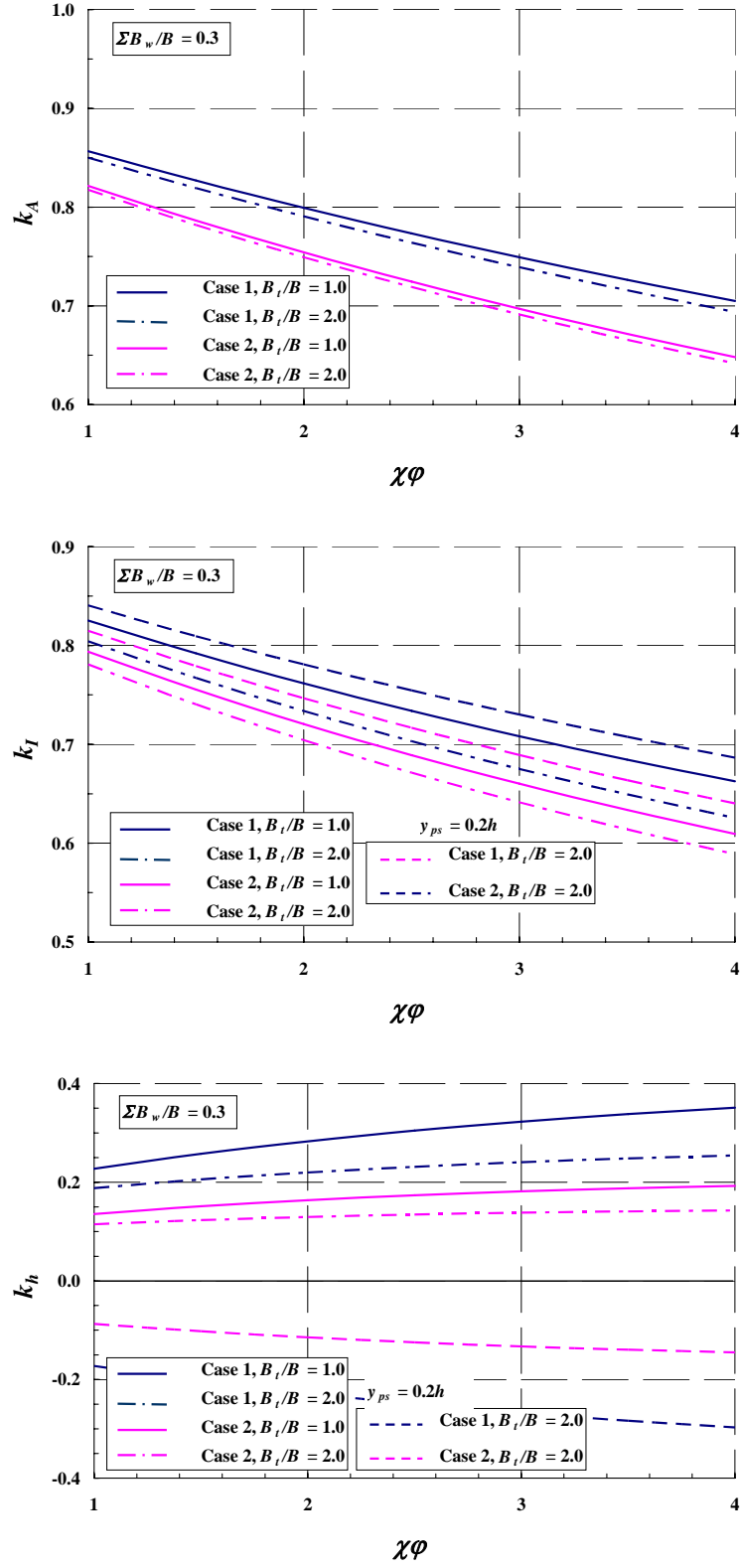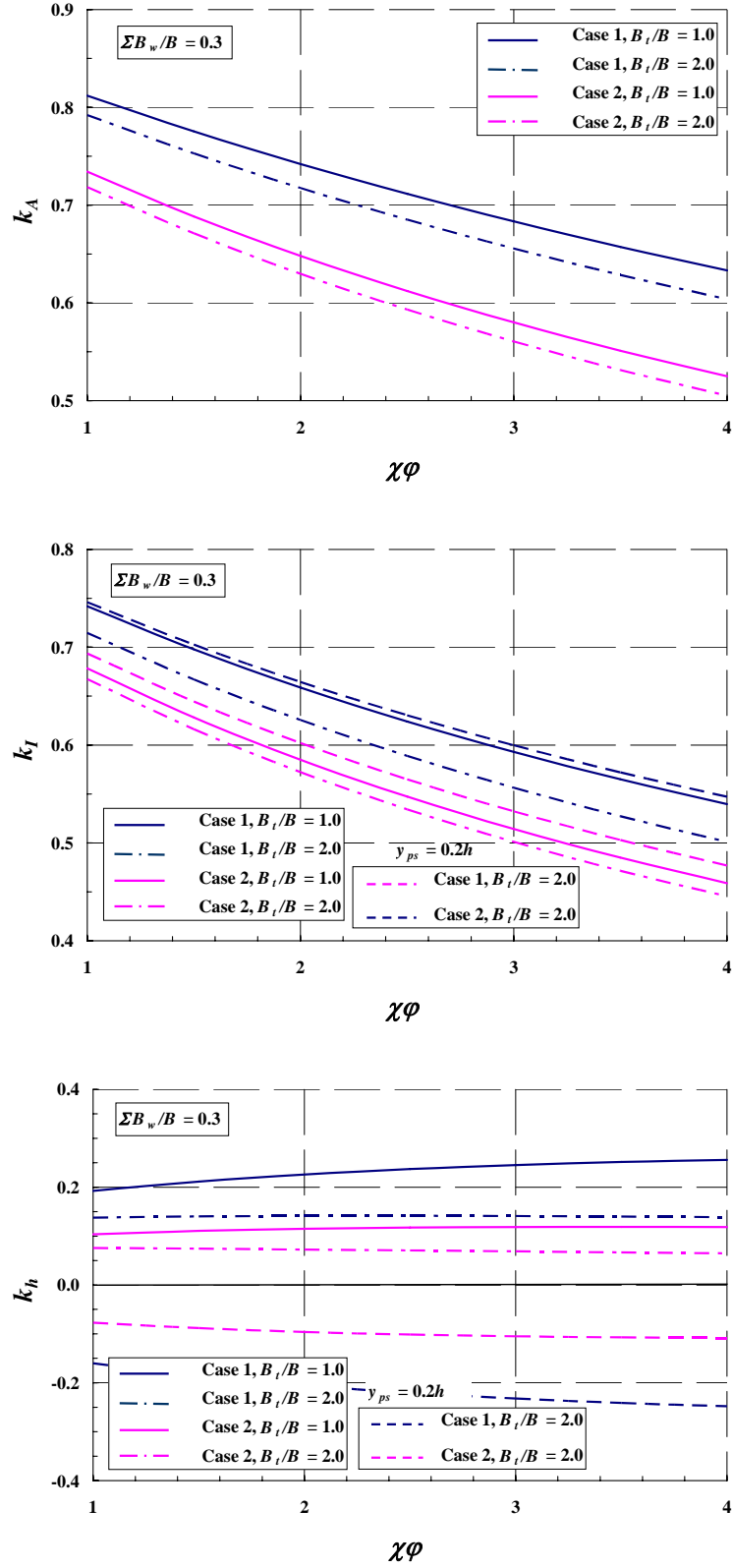
Fig. A.6 k_A, k_I and k_h for the case $\Sigma B_w / B = 0.3$, $\rho_{ns1} = \rho_{ns2} = 1.5\%$, $\rho_{ps} = 0.8\%$.

Fig. A.7 k_A, k_I and k_h for the case $\Sigma B_w/B = 0.1$, $\rho_{ns1} = \rho_{ns2} = 3.0\%$, $\rho_{ps} = 0.8\%$.

Fig. A.8 k_A, k_I and k_h for the case $\Sigma B_w/B = 0.2$, $\rho_{ns1} = \rho_{ns2} = 3.0\%$, $\rho_{ps} = 0.8\%$.

Fig. A.9 k_A, k_I and k_h for the case $\Sigma B_w/B = 0.3$, $\rho_{ns1} = \rho_{ns2} = 3.0\%$, $\rho_{ps} = 0.8\%$.
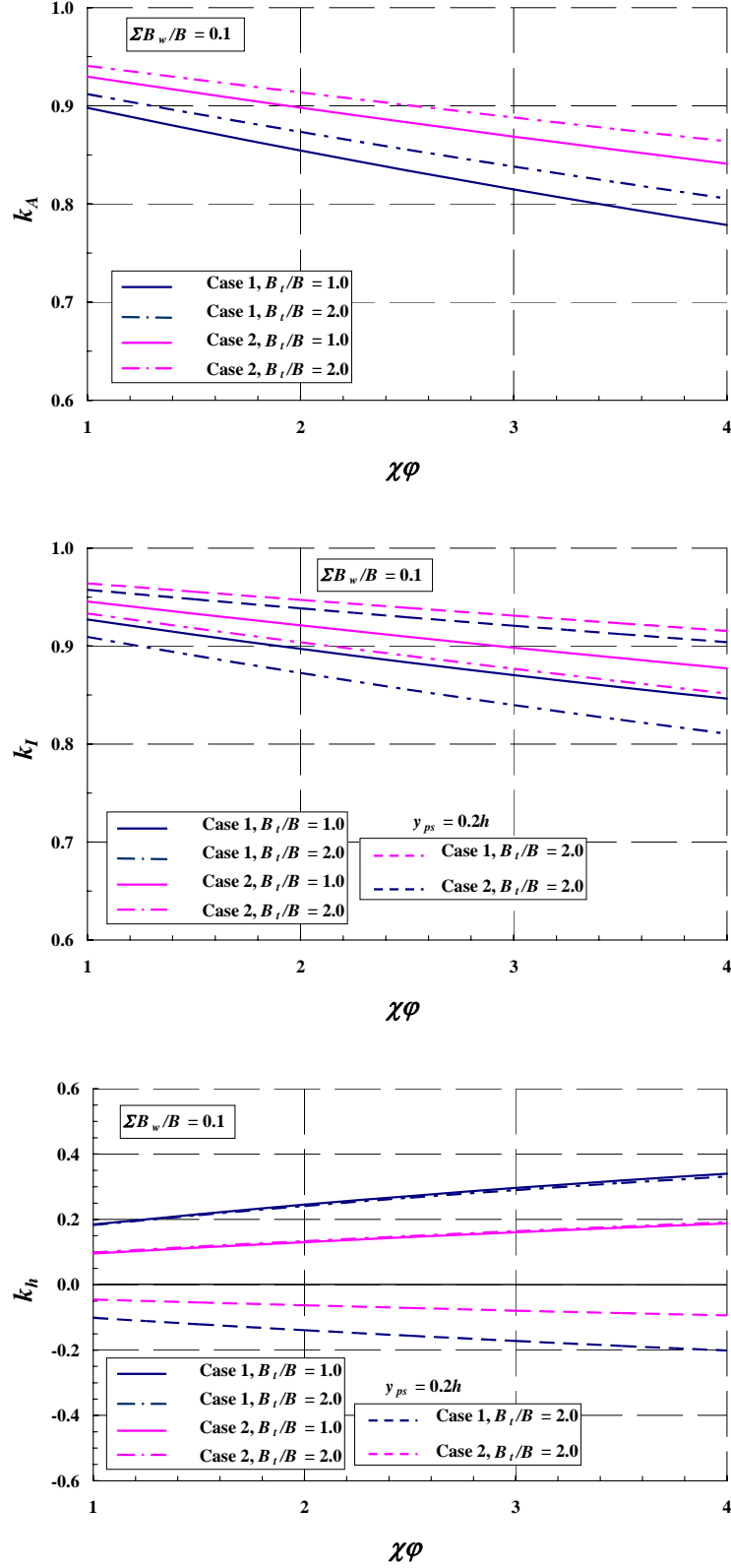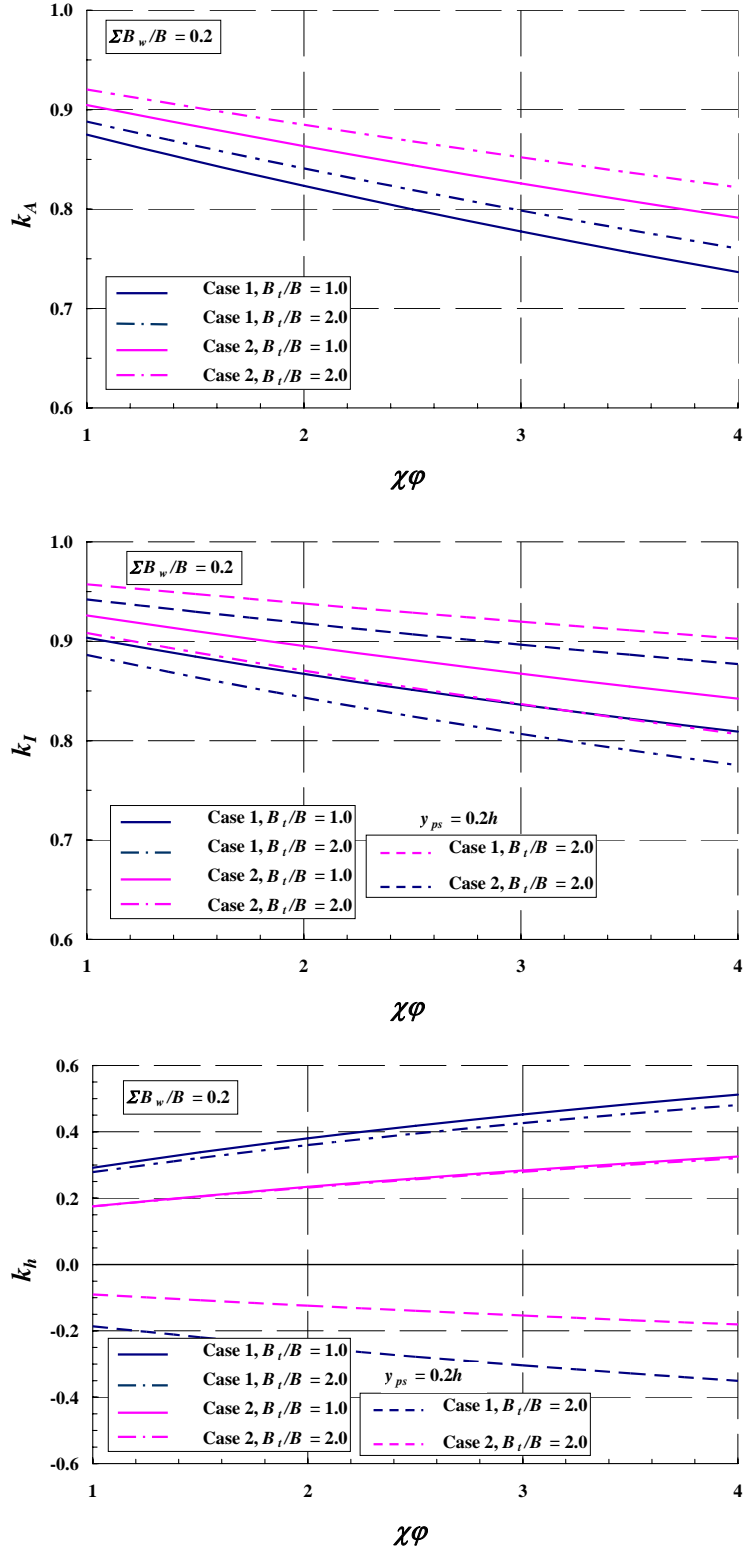
Fig. A.10 k_A, k_I and k_h for the case $\Sigma B_w/B = 0.1$, $\rho_{ns1} = \rho_{ns2} = 0.2\%$, $\rho_{ps} = 1.2\%$.

Fig. A.11 k_A, k_I and k_h for the case $\Sigma B_w/B = 0.2$, $\rho_{ns1} = \rho_{ns2} = 0.2\%$, $\rho_{ps} = 1.2\%$.
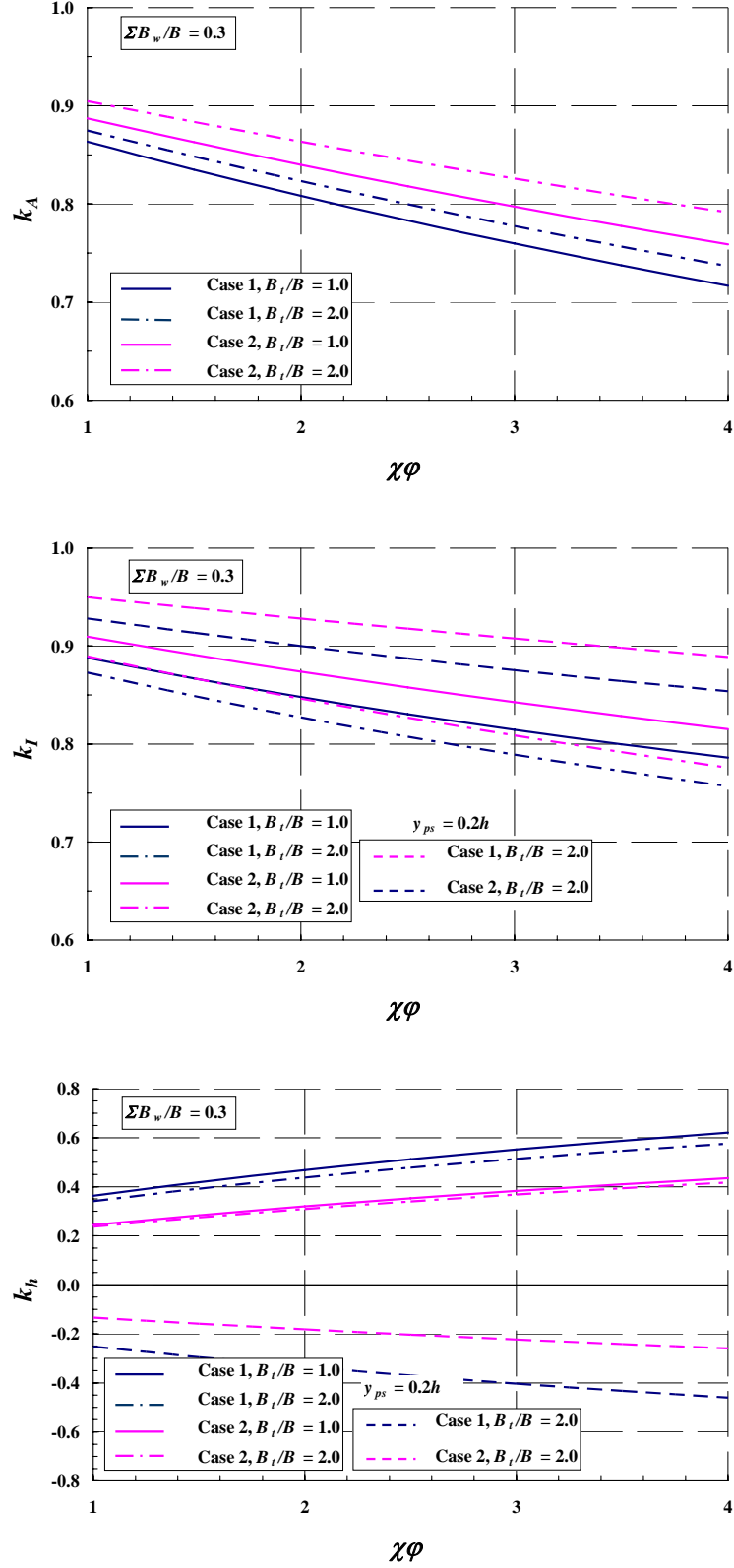
Fig. A.12 k_A, k_I and k_h for the case $\Sigma B_w/B$ =0.3, $\rho_{ns1} = \rho_{ns2} = 0.2\%$, $\rho_{ps} = 1.2\%$.
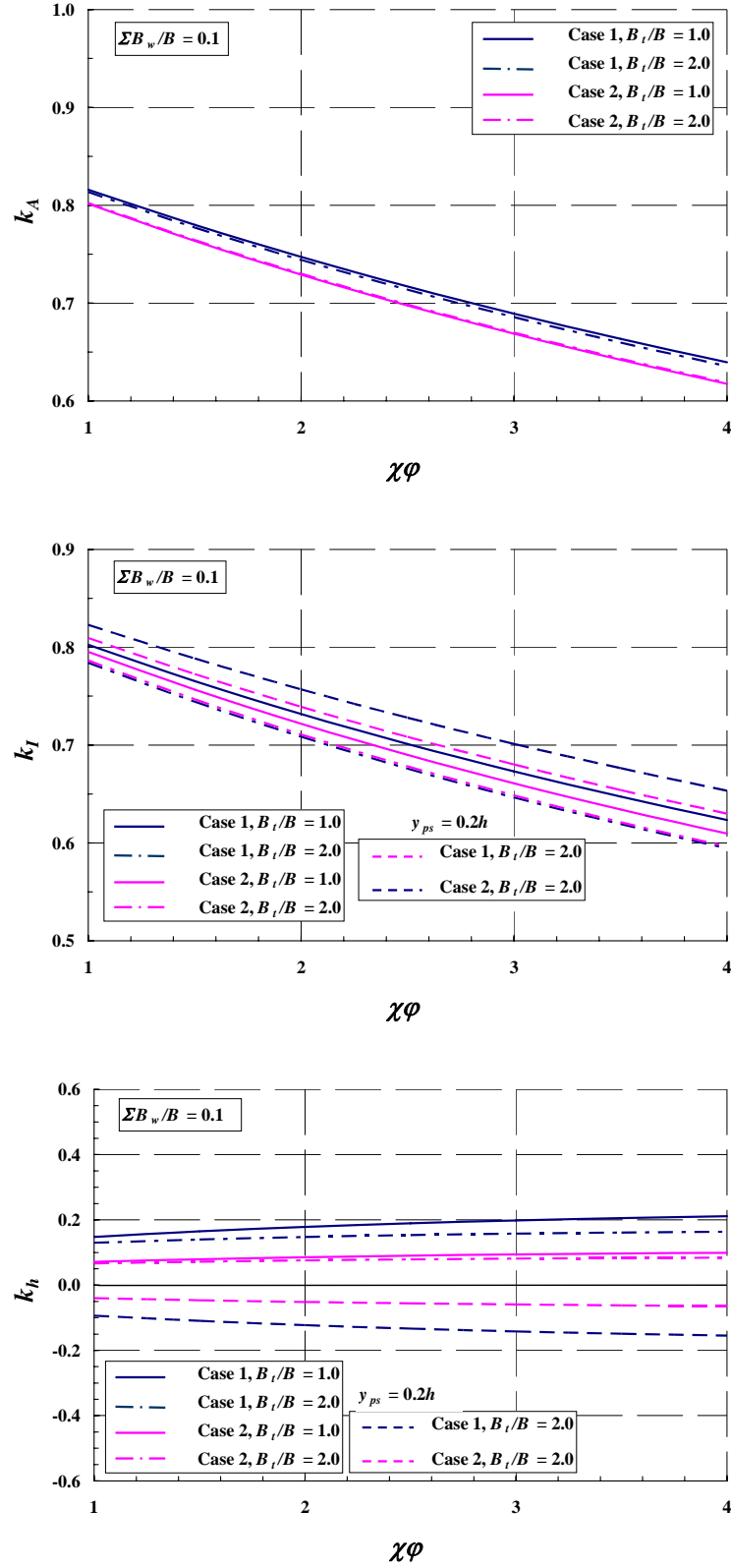
Fig. A.13 k_A, k_I and k_h for the case $\Sigma B_w/B = 0.1$, $\rho_{ns1} = \rho_{ns2} = 1.5\%$, $\rho_{ps} = 1.2\%$.

Fig. A.14 k_A, k_I and k_h for the case $\Sigma B_w/B = 0.2$, $\rho_{ns1} = \rho_{ns2} = 1.5\%$, $\rho_{ps} = 1.2\%$.

Fig. A.15 k_A, k_I and k_h for the case $\Sigma B_w/B = 0.3$, $\rho_{ns1} = \rho_{ns2} = 1.5\%$, $\rho_{ps} = 1.2\%$.
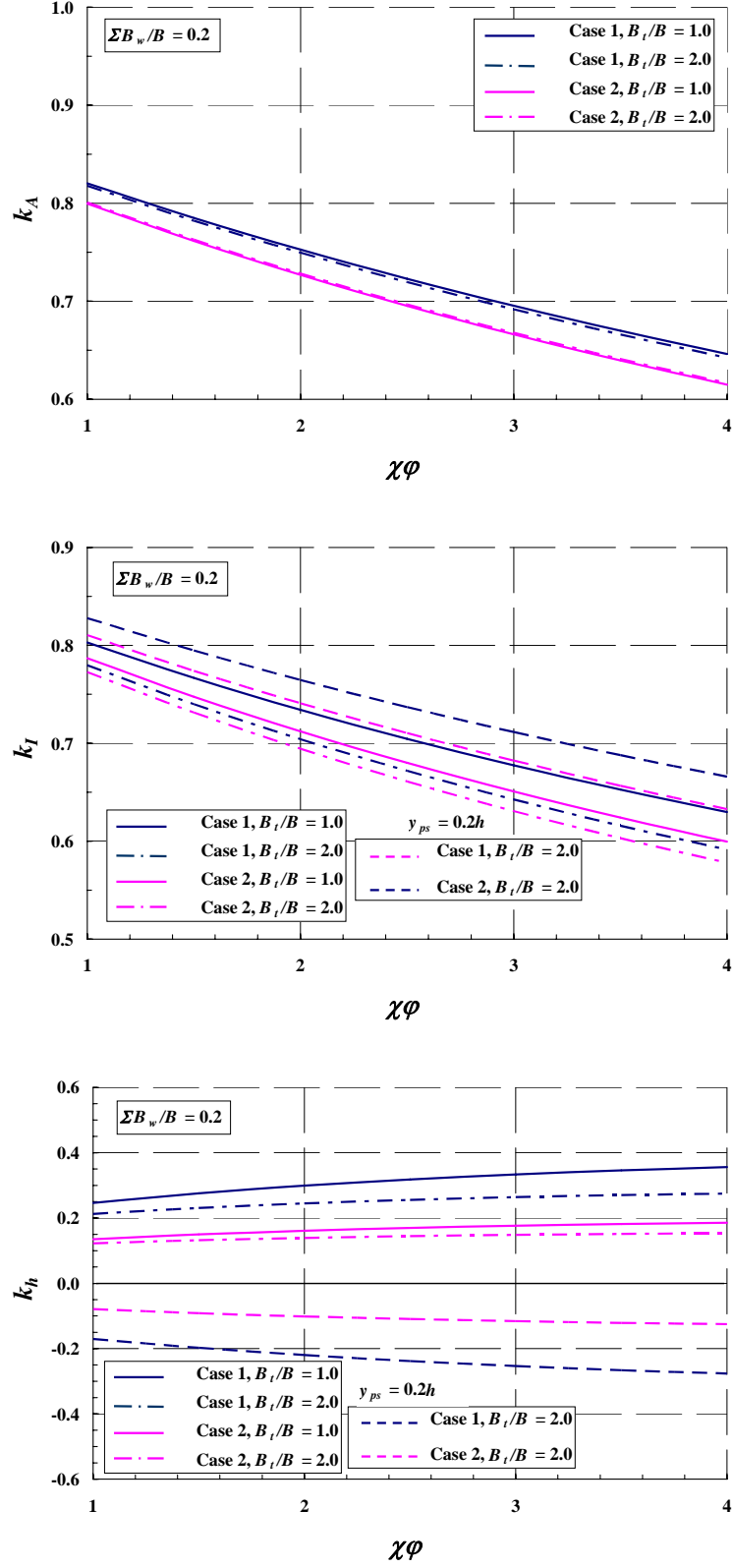
Fig. A.16 k_A, k_I and k_h for the case $\Sigma B_w / B = 0.1$, $\rho_{ns1} = \rho_{ns2} = 3.0\%$, $\rho_{ps} = 1.2\%$.

Fig. A.17 k_A, k_I and k_h for the case $\Sigma B_w/B = 0.2, \rho_{ns1} = \rho_{ns2} = 3.0\%, \rho_{ps} = 1.2\%$.
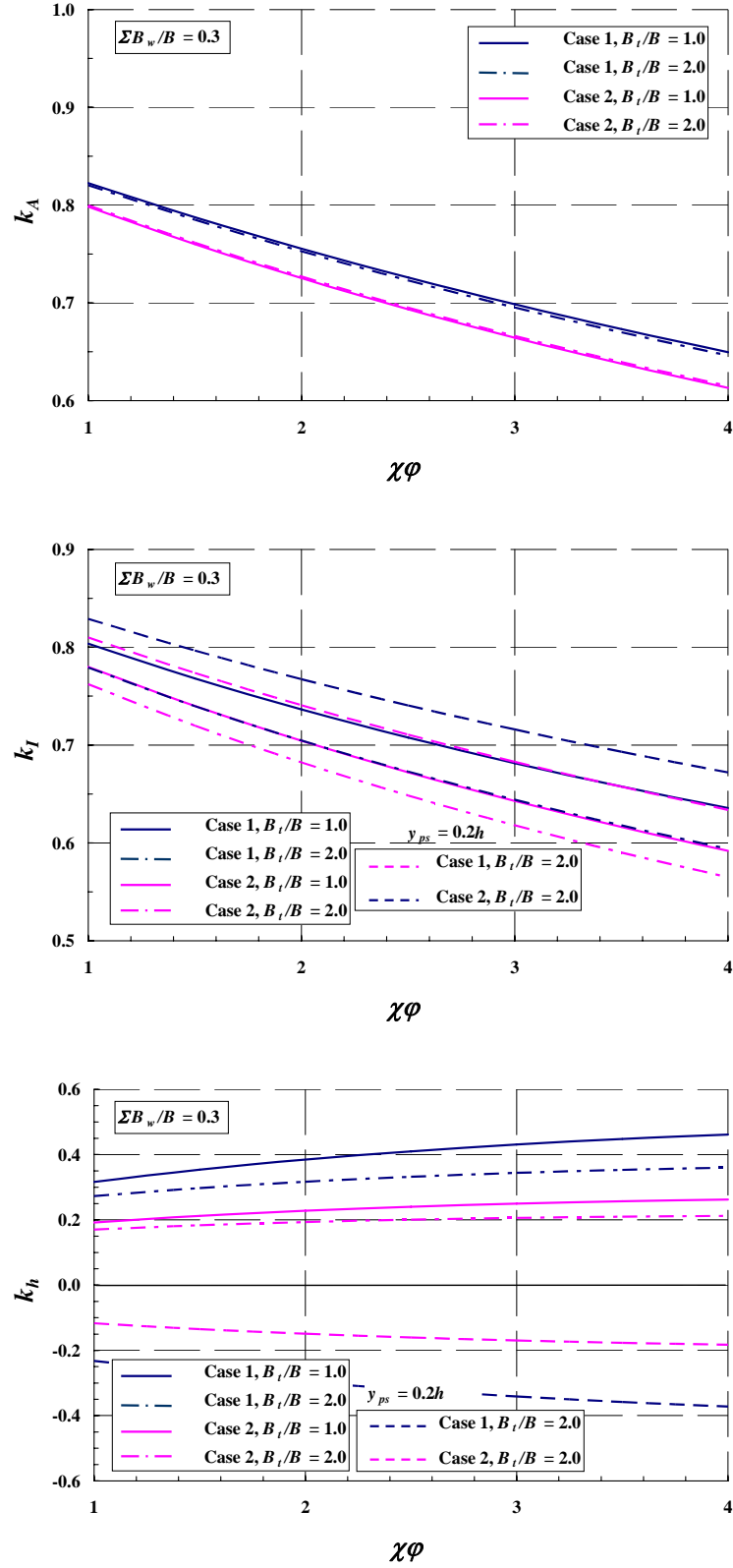
Fig. A.18 k_A, k_I and k_h for the case $\Sigma B_w/B = 0.3$, $\rho_{ns1} = \rho_{ns2} = 3.0\%$, $\rho_{ps} = 1.2\%$.
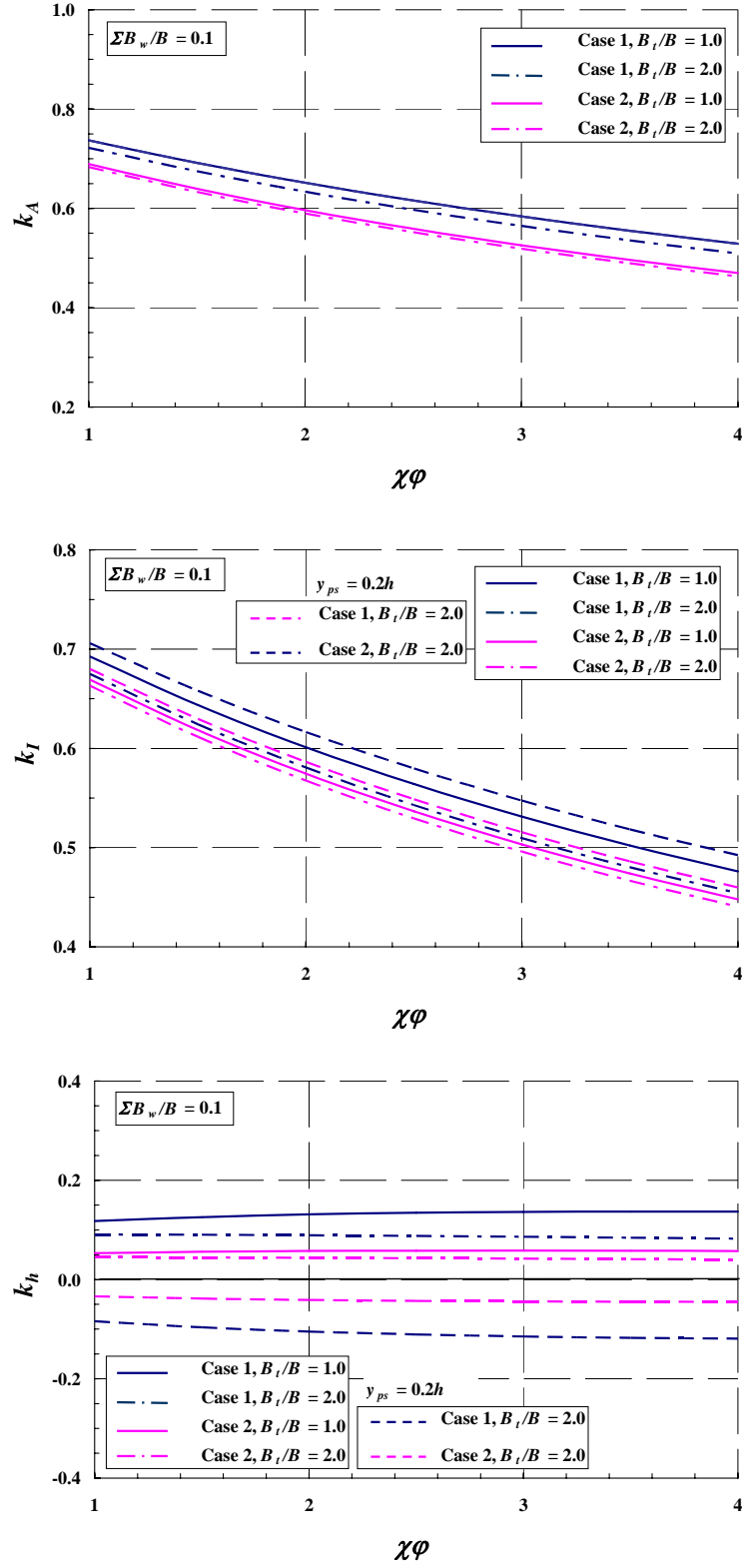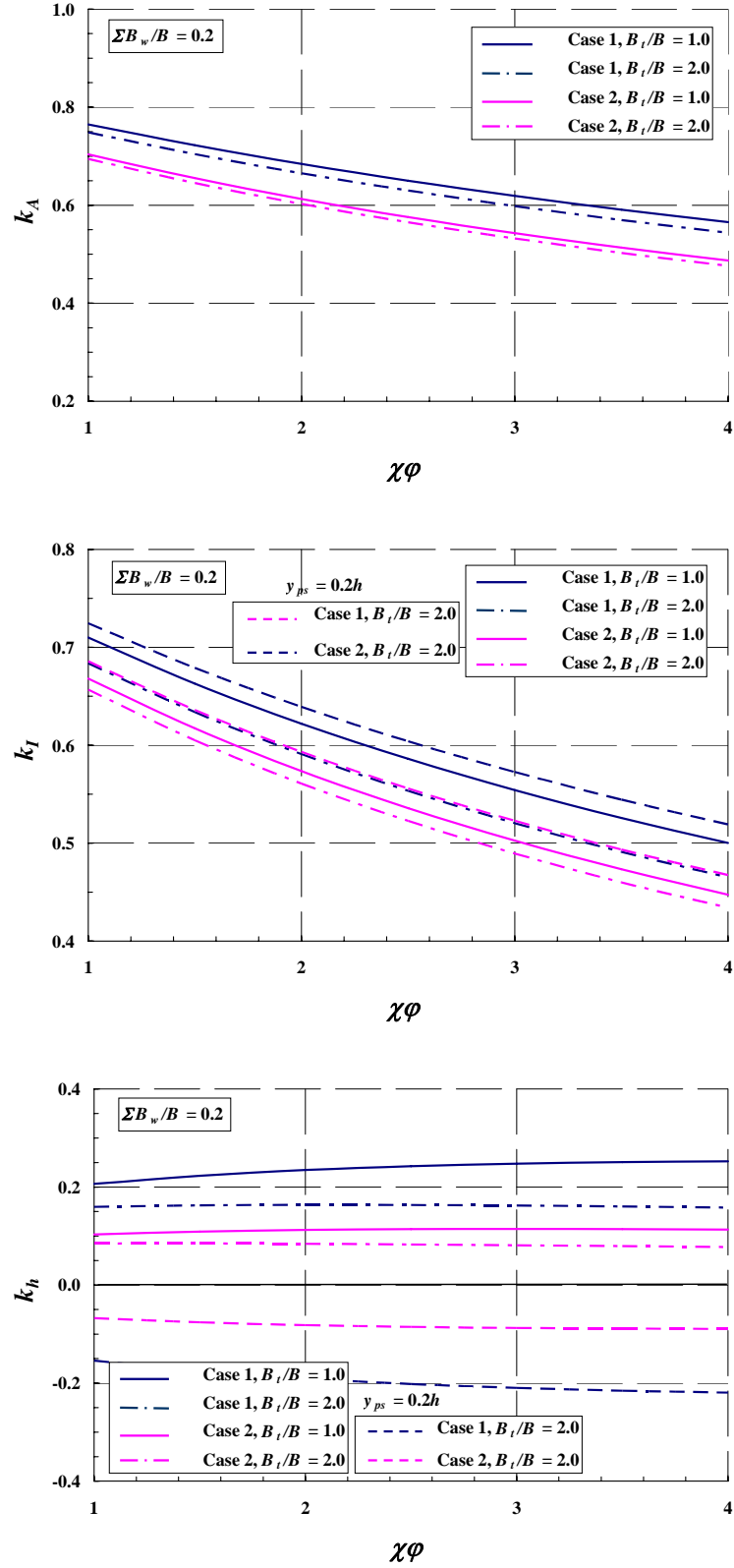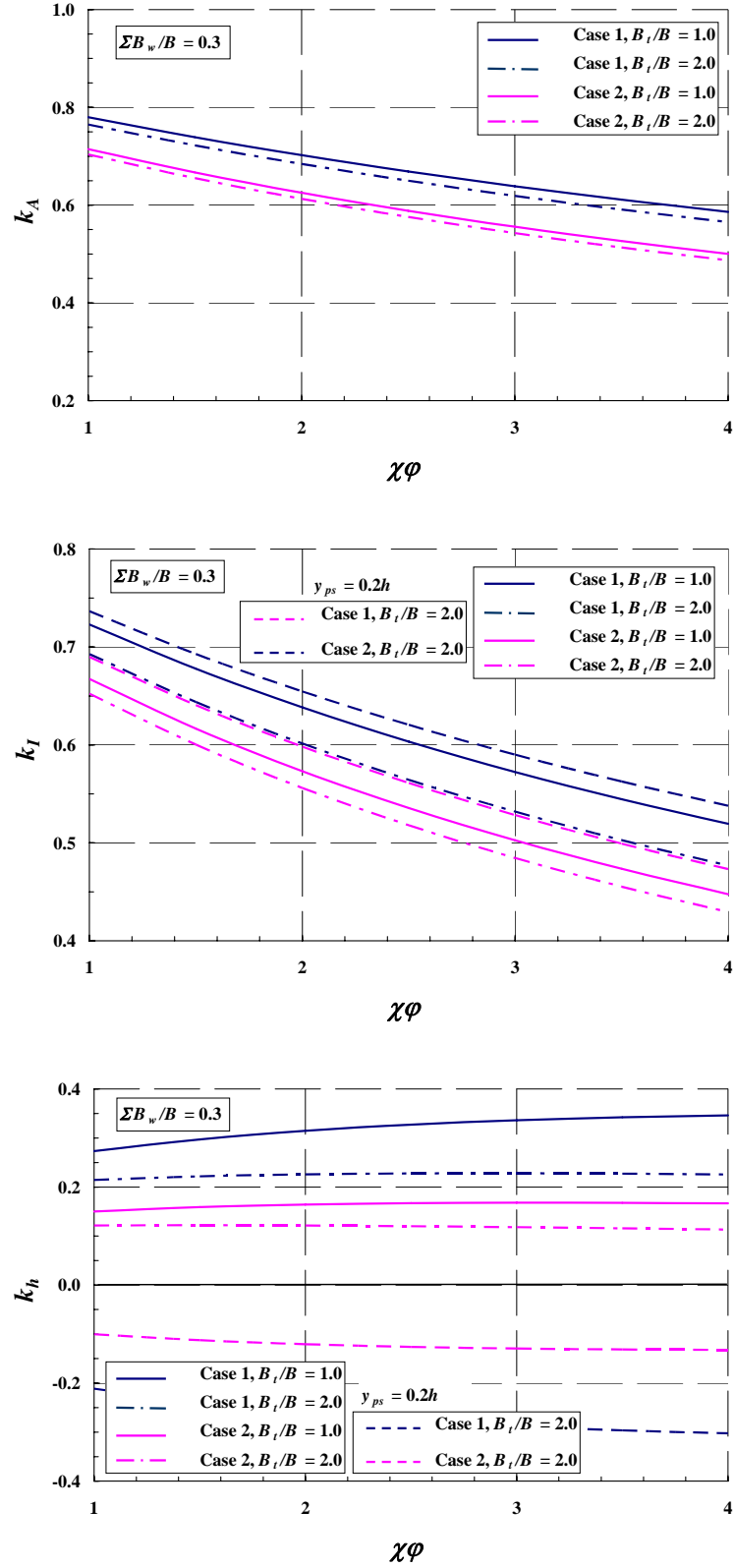
Appendix B: Prestress Loss Due to Continuity

The approach to estimate prestress losses due to continuity in two-unequal-span continuous beam was outlined in Section 4.6. In the following, the approach will be extended to symmetric beams with two to five spans. The coordinate system and locations of integration points (sections) are illustrated in Figs. B.1(a) to (d). The sections are located either at intermediate supports or at mid-spans. In case of four or five spans, the equations are to be solved for two unknows: the connecting moments over intermediate supports ΔF_1 and ΔF_2. The prestress loss due to continuity at each section is evaluated for the combined effect of the values of ΔF_1 and ΔF_2 at this section; see Eqs. B.16 and B.23. For definition of symbols used in the equations, refer to Sec. 4.6.
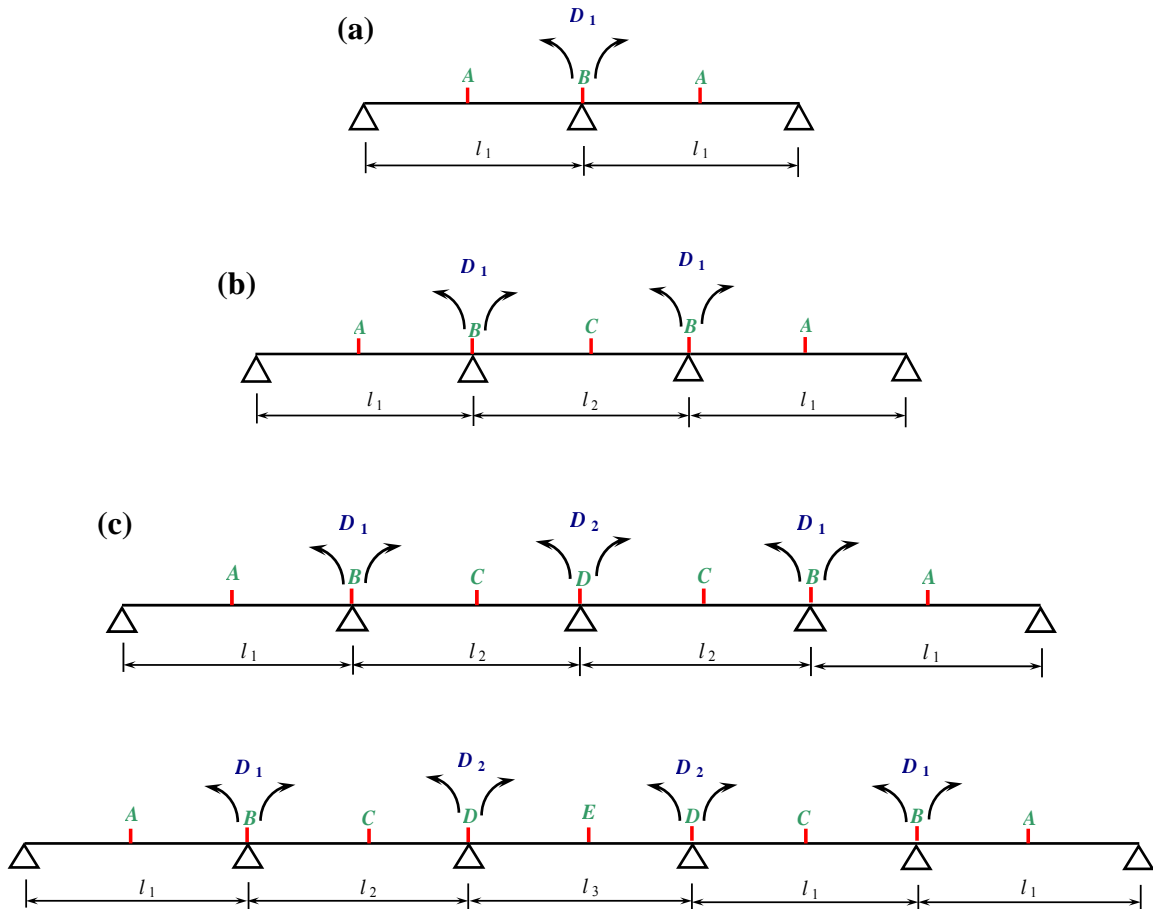

Fig. B.1 Coordinate system and locations of integration points (sections) for continuous beams: (a) two spans; (b) three spans; (c) four spans; and (d) five spans.

(a) Two Spans:

$$\Delta D_1 = \frac{l_1}{3}\left[2(\Delta\psi)_A + (\Delta\psi)_B\right] \tag{B.1}$$

$$\overline{f}_{11} = \frac{l_1}{3}\left[2(\Delta\psi_{u1})_A + (\Delta\psi_{u1})_B\right] \tag{B.2}$$

$$\Delta F_1 = \frac{-\Delta D_1}{\overline{f}_{11}} \tag{B.3}$$

$$\left(\Delta\sigma_{ps(cont)}\right)_i = \left(\frac{E_{ps}}{\overline{E}_c}\right)\left(\frac{\Delta F_1}{\overline{I}}\, y_{ps}\right)_i \tag{B.4}$$

(b) Three Spans:

$$\Delta D_1 = \frac{l_1}{6}\left[2(\Delta\psi)_A + (\Delta\psi)_B\right] + \frac{l_2}{6}\left[2(\Delta\psi)_C + (\Delta\psi)_B\right] \tag{B.5}$$

$$\overline{f}_{11} = \frac{l_1}{6}\left[2(\Delta\psi_{u1})_A + (\Delta\psi_{u1})_B\right] + \frac{l_2}{6}\left[2(\Delta\psi_{u1})_C + (\Delta\psi_{u1})_B\right] \tag{B.6}$$

$$\Delta F_1 = \frac{-\Delta D_1}{\overline{f}_{11}} \tag{B.7}$$

$$\left(\Delta\sigma_{ps(cont)}\right)_i = \left(\frac{E_{ps}}{\overline{E}_c}\right)\left(\frac{\Delta F_1}{\overline{I}}\, y_{ps}\right)_i \tag{B.8}$$

(c) Four Spans:

$$\Delta D_1 = \frac{l_1}{6}\left[2(\Delta\psi)_A + (\Delta\psi)_B\right] + \frac{l_2}{6}\left[2(\Delta\psi)_C + (\Delta\psi)_B\right] \tag{B.9}$$

$$\Delta D_2 = \frac{l_2}{3}\left[2(\Delta\psi)_C + (\Delta\psi)_D\right] \tag{B.10}$$

$$\overline{f}_{11} = \frac{l_1}{6}\left[2(\Delta\psi_{u1})_A + (\Delta\psi_{u1})_B\right] + \frac{l_2}{6}\left[2(\Delta\psi_{u1})_C + (\Delta\psi_{u1})_B\right] \tag{B.11}$$

$$\overline{f}_{22} = \frac{l_2}{3}\left[2(\Delta\psi_{u2})_C + (\Delta\psi_{u2})_D\right] \tag{B.12}$$

$$\overline{f}_{21} = \frac{l_2}{3}\left[2(\Delta\psi_{u1})_C\right] ; \quad \overline{f}_{12} = \frac{l_2}{6}\left[2(\Delta\psi_{u2})_C\right] \tag{B.13}$$

$$\begin{bmatrix} \overline{f}_{11} & \overline{f}_{12} \\ \overline{f}_{21} & \overline{f}_{22} \end{bmatrix} \begin{Bmatrix} \Delta F_1 \\ \Delta F_2 \end{Bmatrix} = - \begin{Bmatrix} \Delta D_1 \\ \Delta D_2 \end{Bmatrix} \tag{B.14}$$

$$\begin{Bmatrix} \Delta F_1 \\ \Delta F_2 \end{Bmatrix} = \frac{1}{\left(\overline{f}_{11} \overline{f}_{22} - \overline{f}_{12} \overline{f}_{21} \right)} \begin{bmatrix} \overline{f}_{22} & -\overline{f}_{12} \\ -\overline{f}_{21} & \overline{f}_{11} \end{bmatrix} \begin{Bmatrix} -\Delta D_1 \\ -\Delta D_2 \end{Bmatrix} \tag{B.15}$$

$$\left(\Delta \sigma_{ps(cont)} \right)_i = \left(\frac{E_{ps}}{\overline{E}_c} \right) \left(\frac{\Delta F_1 + \Delta F_2}{\overline{I}} y_{ps} \right)_i \tag{B.16}$$

(d) Five Spans:

$$\Delta D_1 = \frac{l_1}{6} \left[2(\Delta \psi)_A + (\Delta \psi)_B \right] + \frac{l_2}{6} \left[2(\Delta \psi)_C + (\Delta \psi)_B \right] \tag{B.17}$$

$$\Delta D_2 = \frac{l_2}{6} \left[2(\Delta \psi)_C + (\Delta \psi)_D \right] + \frac{l_3}{6} \left[2(\Delta \psi)_C + (\Delta \psi)_E \right] \tag{B.18}$$

$$\overline{f}_{11} = \frac{l_1}{6} \left[2(\Delta \psi_{u1})_A + (\Delta \psi_{u1})_B \right] + \frac{l_2}{6} \left[2(\Delta \psi_{u1})_C + (\Delta \psi_{u1})_B \right] \tag{B.19}$$

$$\overline{f}_{22} = \frac{l_2}{6} \left[2(\Delta \psi_{u2})_C + (\Delta \psi_{u2})_D \right] + \frac{l_3}{6} \left[2(\Delta \psi_{u2})_C + (\Delta \psi_{u2})_E \right] \tag{B.20}$$

$$\overline{f}_{21} = \frac{l_2}{6} \left[2(\Delta \psi_{u1})_C \right] ; \quad \overline{f}_{12} = \frac{l_2}{6} \left[2(\Delta \psi_{u2})_C \right] \tag{B.21}$$

$$\begin{Bmatrix} \Delta F_1 \\ \Delta F_2 \end{Bmatrix} = \frac{1}{\left(\overline{f}_{11} \overline{f}_{22} - \overline{f}_{12} \overline{f}_{21} \right)} \begin{bmatrix} \overline{f}_{22} & -\overline{f}_{12} \\ -\overline{f}_{21} & \overline{f}_{11} \end{bmatrix} \begin{Bmatrix} -\Delta D_1 \\ -\Delta D_2 \end{Bmatrix} \tag{B.22}$$

$$\left(\Delta \sigma_{ps(cont)} \right)_i = \left(\frac{E_{ps}}{\overline{E}_c} \right) \left(\frac{\Delta F_1 + \Delta F_2}{\overline{I}} y_{ps} \right)_i \tag{B.23}$$